Second-order cyclostationarity-based detection and classification of LTE SC-FDMA signals for cognitive radio

by

©Walid A. Jerjawi

A Thesis submitted to the School of Graduate Studies
in partial fulfilment of the requirements for
the degree of Master of Engineering

Faculty of Engineering and Applied Science
Memorial University of Newfoundland

May 2014

St. John's Newfoundland

Abstract

Cognitive radio (CR) was developed for utilizing the spectrum bands efficiently. Spectrum sensing and awareness represent main tasks of a CR, providing the possibility of exploiting the unused bands.

In this thesis, we investigate the detection and classification of Long Term Evolution (LTE) single carrier-frequency division multiple access (SC-FDMA) signals, which are used in uplink LTE, with applications to cognitive radio. We explore the second-order cyclostationarity of the LTE SC-FDMA signals, and apply results obtained for the cyclic autocorrelation function to signal detection and classification (in other words, to spectrum sensing and awareness). The proposed detection and classification algorithms provide a very good performance under various channel conditions, with a short observation time and at low signal-to-noise ratios, with reduced complexity. The validity of the proposed algorithms is verified using signals generated and acquired by laboratory instrumentation, and the experimental results show a good match with computer simulation results.

Acknowledgements

I would like to thank my supervisors, Dr. Octavia Dobre and Dr. Mohamed Ahmed, from Memorial University of Newfoundland for their suggestions, encouragements, and technical guidance and support which helped me a lot throughout my master's program.

I would also like to thank the students in the Computer Engineering Research Laboratory (CERL) at Memorial University of Newfoundland for the pleasant working environment. Thanks especially to Yahia A. Eldemerdash, who has assisted me in so many ways during my study.

I would like to express gratitude to my brothers and sisters for their encouragement and love over the years.

Finally, and most importantly, I am grateful to my parents. They borned, raised, and supported me. Their endless love and belief in me have been a constant source of inspiration, and this thesis is dedicated to them.

Table of Contents

List of Tables

List of Figures

List of Abbreviations

AWGN ..... Additive white Gaussian noise

CAF ..... Cyclic autocorrelation function

CF ..... Cycle frequency

CP ..... Cyclic prefix

CR ..... Cognitive radio

DL ..... Downlink

DSA ..... Dynamic spectrum access

FCC ..... Federal Communication Commission

FDD ..... Frequency division duplexing

FFT ..... Fast Fourier transform

IFFT ..... Inverse fast Fourier transform

LFDMA .... Localized frequency division multiple access

LTE ..... Long term evolution

OFDM ..... Orthogonal frequency division multiplexing

PAPR ..... Peak-to-average power ratio

PU ..... Primary user

QAM ..... Quadrature amplitude modulation

RRC ..... Root raised cosine

SC-FDMA .. Single carrier-frequency division multiple access

SNR ..... Signal-to-noise ratio

SU ..... Secondary user

TDD ..... Time division duplexing

VSA ..... Vector signal analyzer

VSG ..... Vector signal generator

UL ..... Uplink

List of Symbols

$r(t)$	Continous-time received signal
$w(t)$	Continous-time additive white Gaussian noise
H_0	A null hypothesis, which describes the absence of the signal
H_1	An alternative hypothesis, which describe the presence of the signal
N	FFT size
M	IFFT size
L	Cyclic prefix Length
Q	Expansion factor
$\{x_n^b\}_{n=0}^{N-1}$	The b-th block of input data symbols of SC-FDMA
$\{X_k^b\}_{k=0}^{N-1}$	The frequency domain symbols of SC-FDMA
$\{\tilde{X}_l^b\}_{l=0}^{M-1}$	The output symbols in LFDMA mapping
$\{\tilde{x}_m^b\}_{m=0}^{M-1}$	The time domain symbols of SC-FDMA
$\mathrm{E}[.]$	The expectation operator
$c_r(t,\tau)$	The time-varying autocorrelation function
$c_r(\beta,\tau)$	The cyclic autocorrelation function CAF at CF β and delay τ
$r(n)$	Discrete-time signal
f_s	Sampling rate
$\hat{c}_r(\tilde{\beta},\tilde{\tau})$	The estimator for CAF at CF $\tilde{\beta}$ and delay $\tilde{\tau}$
$g(t)$	The overall impulse response of the transmit and receive filters
τ_s	A fraction of T

c_x	The correlation corresponding to the points in the signal constellation
$\otimes$	Covolution operator
$\Im\{.\}$	Fourier transform
ρ	Oversampling factor
$\tilde{z}_u^b$	The symbol transmitted within the u-th symbol period of block b
$\text{sgn}(\mu)$	The signum function of a real number μ
N_{RB}^{UL}	The number of resource block
N_{SC}^{RB}	The number of subcarriers in a resource block
N_{symb}^{UL}	The consecutive SC-FDMA symbols in the time domain
$\triangle f$	Subcarrier spacing
U_s	Number of samples available at the receive-side
$\hat{\sum}$	Covariance matrix used in the cyclostationarity test
$Q_{2,0}$	Components of the covariance matrix used in the cyclostationarity test
$Q_{2,1}$	Components of the covariance matrix used in the cyclostationarity test
$\hat{Q}_{2,0}$	Estimation of $Q_{2,0}$
$\hat{Q}_{2,1}$	Estimation of $Q_{2,1}$
$f\left(l;\tilde{\tau}_i\right)$	The second-order lag product in the cyclostationarity test
$W^{U_{sw}}$	Spectral window of length U_{sw}
Ψ_1 and Ψ_2	The test statistics used in the cyclostationarity test
Υ	The sum of Ψ_1 and Ψ_2
Γ	Threshold value used in the cyclostationarity test
P_{fa}	The probability of false alarm
P_d	The probability of detection
P_{cc}	The probability of correct classification

Chapter 1

Introduction

1.1 Cognitive Radio

With the increasing demand for high data rate services, which require increased bandwidth, the inadequacy of fixed radio spectrum allocation has become a serious problem. According to the current spectrum assignment policies, a specific band of spectrum is assigned to a certain wireless system. While this resolves the interference problem between different systems, it leads to spectrum scarcity. On the other hand, spectrum is available at various times and geographical locations, and the current assignment basically renders its under-utilization.

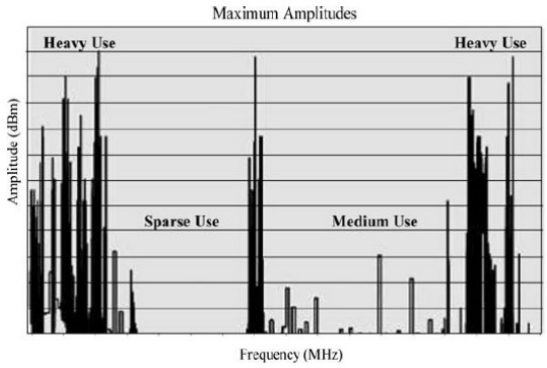

Fig. 1.1: Spectrum usage (taken from [1]).

It has been observed from the measurements depicted in Fig. 1.1 that the utilization of the radio spectrum is not uniform. There is a high activity at some frequencies, but most of the time the spectrum is underutilized. Studies have shown that the utilization of the spectrum ranges from 15% to 85% [2] depending on the time of usage and geographical location. The spectrum is assigned to different operators; this assignment is fixed. This type of allocation technique is known as static allocation. According to the Federal Communications Commission (FCC), the usage of this fixed spectrum is not efficient and creates so-called spectrum-holes or white spaces [3], which refer to time intervals where portions of the frequency spectrum are unused. The above facts make it necessary to start looking for new approaches for spectrum management, outside of the static allocation. Dynamic spectrum access (DSA) refers to communication techniques that exploit the spectrum-holes to increase the spectrum utilization. Cognitive radio (CR) [4] can be seen as one possible approach of implementing DSA that aims to improve spectrum utilization in which the primary (licensed) and the secondary (un-licensed) users co-exist simultaneously. The owner of the channel is referred as the primary user (PU) and all other users are termed as secondary users (SUs) or CR users. SUs are allowed to opportunistically access the spectrum not used by PUs. SUs leave the occupied spectrum when PUs require it. The SUs are then allocated another vacant spectrum, which is not occupied by the PU.

Fig. 1.2 shows a general architecture for a CR network. The components of the CR network architecture can be classified in two groups: the primary network (or licensed network) and the secondary network (or CR network).

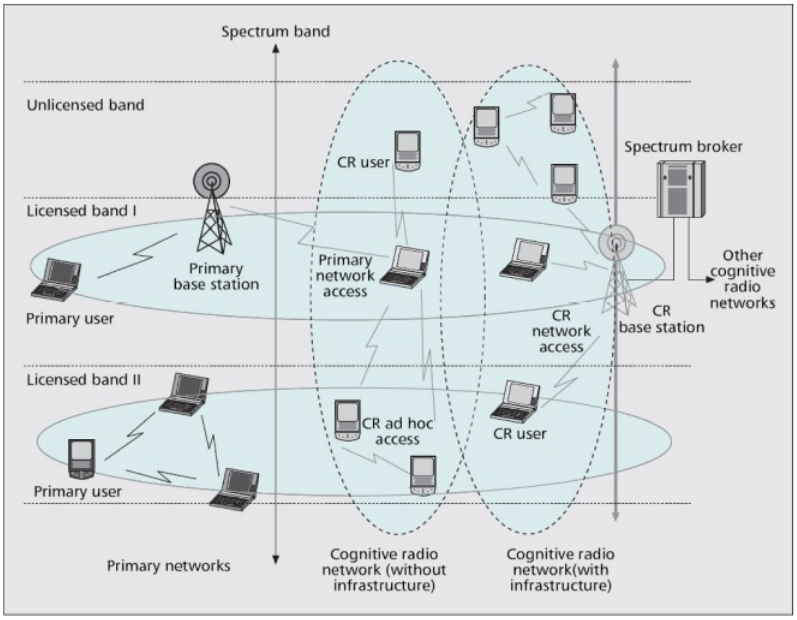

Fig. 1.2: Network architecture for the CR network (taken from [1]).

The primary networks are infrastructured and the users have license to operate in certain spectrum bands. PU activities are controlled through the primary base stations. The secondary network does not have a license to operate in a certain band. CR networks can be equipped with CR base stations that provide a single-hop connection to SUs. CR networks may include spectrum brokers that distribute the spectrum resources among different CR networks.

As shown in Fig. 1.2, the access to the spectrum by SUs is performed opportunistically by using three different access types:

- CR network access: SUs can access their own CR base station on both licensed and unlicensed spectrum bands because all interactions occur inside the CR network.

- CR ad-hoc access: SUs can communicate with other SUs through ad-hoc connections on both licensed and unlicensed spectrum bands.

- Primary network access: SUs can access the primary base station through the licensed band.

1.2 Spectrum Sensing and Awareness

In CR communications, spectrum sensing is performed before an SU starts using the spectrum. By spectrum sensing, the spectrum-holes are determined in order to be used efficiently. There are three major digital signal processing techniques for the detection of the PUs, e.g., the energy detector, the matched filter detector, and the cyclostationary feature detector [1, 2, 5]. In these techniques, weak signals of the PU transmitter are detected on the basis of local observations at the SU. The detection is formulated as a binary hypothesis-testing problem as

$$r(t) = \begin{cases} w(t), & H_0, \\ hs(t) + w(t), & H_1, \end{cases} \tag{1.1}$$

where $r(t)$ is the signal received by the SU, $s(t)$ is the signal transmitted by the PU, $w(t)$ is additive white Gaussian noise (AWGN) and h is the channel amplitude gain. H_0 is the null hypothesis, which describes the absence of the PU in a specific spectrum band. In contrast, H_1 is the alternative hypothesis, which describes the presence of the signal [6].

Energy detection is the most common type of spectrum sensing technique because it is easy to implement and requires no prior knowledge about the PU signal. The energy of the received signal is measured and compared against a threshold to detect the presence of the signal. The disadvantage of the energy detector is that the threshold value depends on the noise level. Therefore, performance of this detector will degrade under noise uncertainty, and detection of weak signals will not be reliably performed.

The matched filter detector is the optimal way for any signal detection, since it maximizes the SNR of the received signal [7]. Its usage is not common in the CR, as it requires prior information about the PUs, such as pulse shaping, packet format, modulation type and order, which is unavailable. The performance could be improved by using pilot symbols, preambles and synchronization codes of the PU signal.

An alternative method for the detection of primary signals is cyclostationary feature detection. Most man-made signals exhibit cyclostationarity, i.e., their time-varying statistics are periodic functions of time. Modulated signals are cyclostationary, with a periodicity related to the symbol period, carrier frequency, or chip rate [1, 2, 5]. On the other hand, the additive Gaussian noise does not exhibit cyclostationarity. This can be employed as a distinctive characteristic to detect the presence of the modulated signals in noise. The cyclostationarity-based methods have the advantage over the matched filter approach of not relying on prior information of the received signal, and have the advantage over the energy detector of being less sensitive to noise uncertainty. In this work, we focus on the cyclostationarity-based approach for signal detection and classification (spectrum sensing and awareness). We should note that in addition to knowing whether a signal is present or not, it is also important for a CR to know the signal type. Based on this information, the SU sets up its transmission parameters. The identification of the type of the signals in the air represents part of spectrum awareness.

Orthogonal frequency division multiplexing (OFDM) represents one of the main candidates for high data rate transmission for current and next generation wireless applications, being adopted by various standards [8–10]. Despite its advantages, it has different disadvantages when employed in the uplink, i.e., the high peak-to-average power ratio (PAPR) and carrier synchronization problems. Hence, single carrier-frequency division multiple access (SC-FDMA) has been introduced as an alternative,

which provides similar performance, efficiency, and low signal processing advantages of OFDM [11]. In addition, it avoids the PAPR and carrier synchronization problems [12]. SC-FDMA has been adopted in the specifications of the long term evolution (LTE) systems [13–15].

Recently, blind signal detection and classification has been intensively studied for OFDM signals. Most of the proposed methods are cyclostationarity-based [10,16–18], with some of them employing the detection of the cyclic prefix (CP)-induced peaks in the CAF [16, 17]. Other methods involve the detection of cyclostationary signatures that are artificially created and intentionally embedded in the OFDM signals [18] by the redundant transmission of message symbols on more than one subcarrier. Subcarrier mapping permits cyclostationary signatures to be embedded in data-carrying waveforms without adding significant complexity to existing transmitter designs. By using this approach, signals can be uniquely classified by the CF created by the embedded signature. However, there is a resultant reduction in the data rate caused by the allocation of subcarriers for signature embedding, when these could otherwise be used for data transmission. Other methods rely on the existence of pilot symbols for channel estimation or synchronization [19]. It is assumed that these symbols are replicated according to a predefined time/frequency distribution, which induces non-zero correlation.

Although detection and classification of OFDM and SC signals have been extensively studied [10, 16–22], to the best of our knowledge there is not such work carried out for SC-FDMA signals. Here we study the second-order cyclostationarity of SC-FDMA signals. The analytical expressions for the cyclic autocorrelation function (CAF) and set of CFs are obtained. Then we employ such findings for the detection of the LTE SC-FDMA signals, as well as for their classification against SC and OFDM signals. Simulations and experiments were carried out, and results reported for signal

detection and classification.

1.3 Thesis Organization

The rest of the thesis is organized as follows.

- Chapter 2 presents the signal model for SC-FDMA signals, the study of second-order cyclostationarity of these signals, and provides closed form expressions for the CAF and CFs of these signals.
- In Chapter 3 we introduce the proposed signal detection algorithm. In addition, performance of this algorithm is investigated by both simulations and experiments.
- In Chapter 4 we present the proposed signal classification algorithm. Simulation and experimental results are presented.
- Chapter 5 provides conclusions and suggestions for future work.

1.4 Major Contributions of the Thesis

- Chapter 2: Signal model for the SC-FDMA signals. The CAF and CF analytical expressions for the SC-FDMA signal [Walid A. Jerjawi et al., *IEEE Tran. on Instrum. Meas.* 2014].
- Chapter 3: Proposed algorithm for signal detection with simulation and experimental results [Walid A. Jerjawi et al., *IEEE Tran. on Instrum. Meas.* 2014].
- Chapter 4: Proposed algorithm for signal classification with simulation and experimental results [Walid A. Jerjawi et al., *IEEE I2MTC* 2014].

Here, we present the publications out of this work:

- Walid A. Jerjawi, Yahia A. Eldemerdash, and Octavia A. Dobre "Blind recognition of SC-FDMA signals using second-order cyclostationarity," accepted to *IEEE I2MTC,* 2014.

- Walid A. Jerjawi, Yahia A. Eldemerdash, and Octavia A. Dobre "Second-order cyclostationarity-based detection of LTE SC-FDMA signals for cognitive radio," submitted to *IEEE Tran. on Instrum. Meas.,* 2014.

Chapter 2

Second-Order Cyclostationarity of the SC-FDMA-based LTE Signals

2.1 Introduction

SC-FDMA signals have been proposed as a promising alternative to OFDM for uplink traffic in LTE systems due to the lower peak-to-average power ratio. On the other hand, they offer the same degree of inter-symbol interference combat as OFDM signals. In this chapter, a model of SC-FDMA signals is presented. Then, their second-order cyclostationarity is studied and closed form expression for the CAF and corresponding set of CFs are derived. Moreover, the CAF results obtained from both analytical findings and computer simulations are presented. Finally, a description of the structure of the LTE SC-FDMA signals is presented.

2.2 SC-FDMA Signal Model

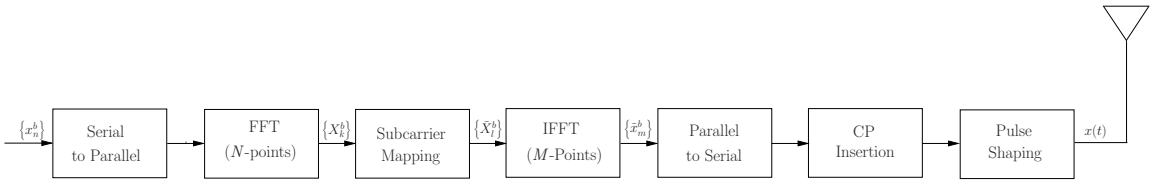

Fig. 2.1: SC-FDMA signal generation [23].

Fig. 2.1 shows the generation of SC-FDMA signals. The b-th block of input data symbols $\{x_n^b\}_{n=0}^{N-1}$ has one of several possible modulation formats, such as QPSK, 16-QAM, and 64-QAM. The serially modulated data symbols are converted into N parallel data streams and passed through an N-point fast Fourier transform (FFT) block, which generates the frequency domain symbols $\{X_k^b\}_{k=0}^{N-1}$. Then, the output of the FFT is passed through the subcarrier mapping block. This assigns the $\{X_k^b\}_{k=0}^{N-1}$ symbols to $M \geq N$ subcarriers, usually in a localized mode (LFDMA) [23]. Note that $M = NQ$, with Q as the expansion factor and the unoccupied subcarriers are set to zero. The output symbols in LFDMA, $\{\tilde{X}_l^b\}_{l=0}^{M-1}$, are frequency domain samples, which can be described as

$$\tilde{X}_l^b = \begin{cases} X_l^b, & 0 \leq l \leq N-1, \\ \\ 0, & N \leq l \leq M-1. \end{cases} \tag{2.1}$$

Fig. 2.2 shows an example of SC-FDMA transmit symbols using the LFDMA subcarrier mapping mode, with $N = 4$, $Q = 2$, and $M = 8$.

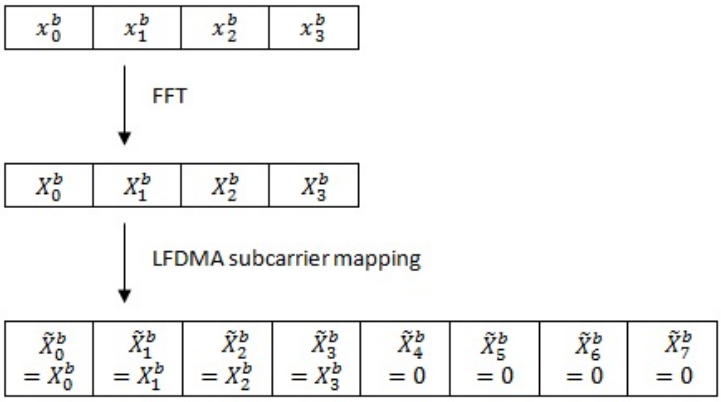

Fig. 2.2: An example of SC-FDMA transmit symbols in frequency domain, using LFDMA subcarrier mapping for $N = 4$, $Q = 2$, and $M = 8$.

The frequency domain samples are passed through an M-point[1] inverse FFT (IFFT) operation, and the time domain symbols $\{\tilde{x}_m^b\}_{m=0}^{M-1}$ can be described as follows [12].

$$\begin{aligned} \tilde{x}_m^b = \tilde{x}_{Qn+q}^b &= \tfrac{1}{M} \sum_{l=0}^{M-1} \tilde{X}_l^b e^{j2\pi \frac{m}{M} l} \\ &= \tfrac{1}{QN} \sum_{l=0}^{N-1} X_l^b e^{j2\pi \frac{Qn+q}{QN} l}, \end{aligned} \tag{2.2}$$

where $m = Qn + q$, $0 \le n \le N-1$, and $0 \le q \le Q-1$.

If $q = 0$, then (2.2) becomes

$$\begin{aligned} \tilde{x}_m^b = \tilde{x}_{Qn}^b &= \tfrac{1}{QN} \sum_{l=0}^{N-1} X_l^b e^{j2\pi \frac{n}{N} l} \\ &= \tfrac{1}{Q} x_n^b. \end{aligned} \tag{2.3}$$

If $q \neq 0$, (2.2) becomes [12]

[1]Note that M is assumed an even integer, according to the common practice for the FFT/IFFT, as well as the wireless communications standards [24–26].

$$\begin{aligned}
\tilde{x}_m^b = \tilde{x}_{Qn+q}^b = \tfrac{1}{QN}\sum_{l=0}^{N-1} X_l^b e^{j2\pi\frac{Qn+q}{QN}l} &= \tfrac{1}{QN}\sum_{l=0}^{N-1}\left(\sum_{p=0}^{N-1} x_p^b e^{-j2\pi\frac{p}{N}l}\right)e^{j2\pi\frac{Qn+q}{QN}l} \\
&= \tfrac{1}{QN}\sum_{l=0}^{N-1}\sum_{p=0}^{N-1} x_p^b e^{j2\pi\left(\frac{(n-p)}{N}+\frac{q}{QN}\right)l} \\
&= \tfrac{1}{QN}\sum_{p=0}^{N-1} x_p^b\left(\sum_{l=0}^{N-1} e^{j2\pi\left(\frac{(n-p)}{N}+\frac{q}{QN}\right)l}\right) \\
&= \tfrac{1}{QN}\sum_{p=0}^{N-1} x_p^b \tfrac{1-e^{j2\pi(n-p)}e^{j2\pi\frac{q}{Q}}}{1-e^{j2\pi\left(\frac{(n-p)}{N}+\frac{q}{QN}\right)}} \\
&= \tfrac{1}{QN}\sum_{p=0}^{N-1} x_p^b \tfrac{1-e^{j2\pi\frac{q}{Q}}}{1-e^{j2\pi\left(\frac{(n-p)}{N}+\frac{q}{QN}\right)}} \\
&= \tfrac{1}{Q}\left(1-e^{j2\pi\frac{q}{Q}}\right)\tfrac{1}{N}\sum_{p=0}^{N-1}\tfrac{x_p^b}{1-e^{j2\pi\left(\frac{(n-p)}{N}+\frac{q}{QN}\right)}}.
\end{aligned} \tag{2.4}$$

As one can see from (2.3), the time domain LFDMA signal samples in the N-multiple sample positions consist of copies of the input time symbols scaled by a factor of 1/Q. Furthermore, from (2.4) it can be noticed that in between these positions, the signal samples are the weighted sums of the time symbols in the input block.

To sum up, the SC-FDMA samples can be expressed in time domain as

$$\tilde{x}_m^b = \begin{cases} \frac{1}{Q}x_n^b, & m = nQ,\ n = 0,\ 1, \ldots,\ N-1, \\ \frac{1}{Q}\left(1-e^{j\frac{2\pi q}{Q}}\right)\frac{1}{N}\sum_{p=0}^{N-1}\frac{x_p^b}{1-e^{j2\pi\left(\frac{(n-p)}{N}+\frac{q}{QN}\right)}}, & m = nQ+q,\ n = 0,\ 1, ..., N-1, \\ & q = 1, \ldots, Q-1. \end{cases} \tag{2.5}$$

Fig. 2.3 shows an example of the LFDMA signal for N=4, Q=2, and M=8. Note that y_i^b represents $\tilde{x}_m^b$, with $i = \frac{m-1}{2}$, $m = Qn+q$, and $q \neq 0$.

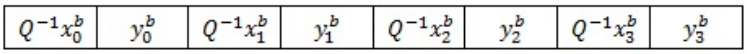

Fig. 2.3: An example of SC-FDMA transmit symbols in time domain using LFDMA subcarrier mapping for N=4, Q=2, and M=8.

At the receiver, the SC-FDMA noise-free signal is expressed as[2]

$$r_{\text{SC-FDMA}}(t) = \sum_{b=-\infty}^{\infty} \sum_{m=0}^{M-1} \tilde{x}_m^b g(t - mT - bMT), \tag{2.6}$$

where b is the block index, m is the symbol index within a block, $\tilde{x}_m^b$ is the symbol transmitted within the m-th symbol period of block b, T is the symbol duration, and $g(t)$ is the overall impulse response of the transmit and receive filters.

2.3 Second-Order Signal Cyclostationarity: Definitions

A random process $r(t)$ is said to be second-order cyclostationary if its mean and time-varying autocorrelation function (AF) are almost periodic functions of time [27]. The latter is expressed as a Fourier series as [27]

$$c_r(t, \tau) = \text{E}[r(t)r^*(t - \tau)] = \sum_{\beta \in \kappa} c_r(\beta, \tau) e^{j2\pi\beta t}, \tag{2.7}$$

where E[.] represents the expectation operator, the superscript * denotes complex conjugation, and $c_r(\beta, \tau)$ is the second-order cyclic autocorrelation function (CAF) at cycle frequency (CF) β and delay τ, which can be expressed as [27]

[2]Note that for the simplicity of the analysis, the noise-free signal is considered here. The noise and channel effects will be taken into account in Chapters 4 and 5.

$$c_r(\beta,\tau) = \lim_{I\to\infty} I^{-1} \int_{-I/2}^{I/2} c_r(t,\tau) e^{-j2\pi\beta t}\, dt, \tag{2.8}$$

and $\kappa = \{\beta : c_r(\beta,\tau) \neq 0\}$ represents the set of CFs.

A discrete-time signal $r(n)$ is obtained by periodically sampling the continous-time signal $r(t)$ at rate f_s, and its CAF at CF $\tilde{\beta}$ and delay $\tilde{\tau}$ is given by[3] [27]

$$c_r(\tilde{\beta},\tilde{\tau}) = c_r(\beta f_s^{-1}, \tau f_s). \tag{2.9}$$

The estimator for CAF at CF $\tilde{\beta}$ and delay $\tilde{\tau}$, based on U_s samples, is given by [27]

$$\hat{c}_r(\tilde{\beta},\tilde{\tau}) = \frac{1}{U_s} \sum_{u=0}^{U_s-1} r(u) r^*(u-\tilde{\tau}) e^{-j2\pi\tilde{\beta}u}. \tag{2.10}$$

2.4 AF, CAF, and Set of CFs for the SC-FDMA Signals

The AF of the SC-FDMA signal can be expressed as

$$c_r(t,\tau) = \mathrm{E}\left[r_{\text{SC-FDMA}}(t) r^*_{\text{SC-FDMA}}(t-\tau)\right]. \tag{2.11}$$

Therefore, by using (2.6), (2.11) can be written as

$$c_r(t,\tau) = \sum_{b_1=-\infty}^{\infty} \sum_{b_2=-\infty}^{\infty} \sum_{m_1=0}^{M-1} \sum_{m_2=0}^{M-1} \mathrm{E}\left[\tilde{x}_{m_1}^{b_1} (\tilde{x}_{m_2}^{b_2})^*\right] g(t-m_1T-b_1MT) g^*(t-m_2T-b_2MT-\tau), \tag{2.12}$$

where $\tau = \mu T + \tau_s$, $\mu = \pm 1, \pm 2, ..., \pm(M-1)$, with τ_s as a fraction of T $(0 \leq \tau_s \leq T)$.

Based on (2.5) and (2.12), the AF of the SC-FDMA signal is investigated in the

[3]Note that these results are valid under the assumption of no aliasing in cyclic and spectral frequency domains.

following cases[4]:

Case (1): Zero delay ($\tau = 0$)

Here we derive the analytical expression for the AF at delay equal to zero. This case is illustrated in Fig. 2.4.

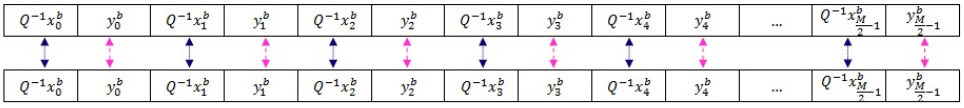

Fig. 2.4: SC-FDMA symbols for $\tau = 0$.

From (2.12), one can notice that $c_r(t,0)$ has non-zero significant values when $b_1 = b_2 = b$ (the same data block) and $m_1 = m_2 = m$ (the same symbol within a block). Based on this observation, (2.12) can be expressed as

$$c_r(t;0) = \sum_{b=-\infty}^{\infty} \sum_{m=0}^{M-1} \mathrm{E}\left[\tilde{x}_m^b (\tilde{x}_m^b)^*\right] g(t - mT - bMT) g^*(t - mT - bMT). \tag{2.13}$$

In this case, we split the sum over m in (2.13) into two sums[4]: the first one is over m (even) $= 2n$, $n = 0, ..., N-1$, and the second one is over m (odd)$= 2n+1$, $n = 0, ..., N-1$. Therefore (2.13) becomes

$$\begin{aligned} c_r(t;0) = & \overbrace{\sum_{b=-\infty}^{\infty} \Big(\sum_{\substack{m=0 \\ \text{even}}}^{M-1} \mathrm{E}[\tilde{x}_m^b (\tilde{x}_m^b)^*] g(t - mT - bMT) g^*(t - mT - bMT) \Big)}^{\mathfrak{c}_r^{(1)}(t;0)} \\ & + \overbrace{\sum_{b=-\infty}^{\infty} \Big(\sum_{\substack{m=0 \\ \text{odd}}}^{M-1} \mathrm{E}\left[\tilde{x}_m^b (\tilde{x}_m^b)^*\right] g(t - mT - bMT) g^*(t - mT - bMT) \Big)}^{\mathfrak{c}_r^{(2)}(t;0)}. \end{aligned} \tag{2.14}$$

Furthermore, by replacing (2.5) into (2.14), and with $Q = 2$, $\mathfrak{c}_r^{(1)}(t;0)$ becomes

[4]With the signal model in (2.5), we consider $Q = 2$ for illustration. As such, $q = 0, 1$.

$$\begin{aligned}\mathfrak{c}_r^{(1)}(t;0) &= \tfrac{1}{4}\sum_{b=-\infty}^{\infty}\sum_{\substack{m=0\\ m=2n,\,even\\ n=0,\ldots,N-1}}^{M-1}\mathrm{E}[x_n^b(x_n^b)^*]g(t-mT-bMT)g^*(t-mT-bMT)\\ &= \tfrac{c_x}{4}\sum_{b=-\infty}^{\infty}\sum_{\substack{m=0\\ m=2n,\,even\\ n=0,\ldots,N-1}}^{M-1}g(t-mT-bMT)g^*(t-mT-bMT),\end{aligned} \tag{2.15}$$

where $c_x = \mathrm{E}[x_n^b(x_n^b)^*]$ represents the correlation corresponding to the points in the signal constellation.

By replacing (2.5) into (2.14), and with $Q = 2$, $\mathfrak{c}_r^{(2)}(t;0)$ becomes

$$\begin{aligned}\mathfrak{c}_r^{(2)}(t;0) &= \sum_{b=-\infty}^{\infty}\sum_{\substack{m=0\\ m=2n+1,\,odd\\ n=0,\ldots,N-1}}^{M-1}\left(\tfrac{1}{2N}\left(1-e^{j\pi}\right)\right)^2\\ &\quad\times\mathrm{E}\left[\sum_{p=0}^{N-1}\frac{x_p^b(x_p^b)^*}{\left(1-e^{j2\pi\left(\frac{(n-p)}{N}+\frac{1}{2N}\right)}\right)\left(1-e^{-j2\pi\left(\frac{(n-p)}{N}+\frac{1}{2N}\right)}\right)}\right]\\ &\quad\times g(t-mT-bMT)g^*(t-mT-bMT))\\ &= \tfrac{c_x}{2N^2}\sum_{b=-\infty}^{\infty}\sum_{\substack{m=0\\ m=2n+1,\,odd\\ n=0,\ldots,N-1}}^{M-1}\left[\sum_{p=0}^{N-1}\frac{1}{1-\cos\left(\pi\left(\frac{2n-2p+1}{N}\right)\right)}\right]\\ &\quad\times g(t-mT-bMT)g^*(t-mT-bMT).\end{aligned} \tag{2.16}$$

By evaluating the summation $\sum_{p=0}^{N-1}\frac{1}{1-\cos\left(\pi\left(\frac{2n-2p+1}{N}\right)\right)}$ through numerical calculations, we found that it equals $\frac{N^2}{2}$.

Therefore, (2.16) becomes

$$\mathfrak{c}_r^{(2)}(t;0) = \frac{c_x}{4}\sum_{b=-\infty}^{\infty}\sum_{\substack{m=0\\ \text{odd}}}^{M-1}g(t-mT-bMT)g^*(t-mT-bMT). \tag{2.17}$$

By substituting (2.15) and (2.17) in (2.14), we obtain

$$c_r(t;0) \;\; = \tfrac{c_x}{4} \sum_{b=-\infty}^{\infty} \sum_{m=0}^{M-1} g(t-mT-bMT)g^*(t-mT-bMT), \tag{2.18}$$

and with $k = bM + m$, the AF can be further written as

$$c_r(t;0) = \frac{c_x}{4}\left[g(t)g^*(t)\right] \otimes \sum_{k=-\infty}^{\infty} \delta(t-kT). \tag{2.19}$$

Case (2): Delay $\tau = \mu T + \tau_s$, $\mu = \pm 1, \pm 3, ..., \pm(M-1)$ (odd integer), $\tau_s = 0$

In the following, we derive the analytical expression for the AF at $\tau =$ delay μT, $\mu = \pm 1, \pm 3, \pm(M-1)$. An example is provided in Fig. 2.5 for $\mu = 1$.

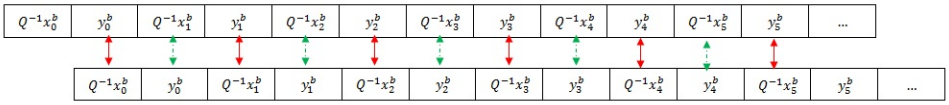

Fig. 2.5: SC-FDMA symbols for $\mu = 1$.

In this case, there are two types of terms in the AF in (2.12): 1) when the symbols belong to the same data block $b_1 = b_2$ (the corresponding term in $c_r(t;0)$ is denoted by $\mathfrak{c}_r^{(1)}(t;\tau)$), 2) when the symbols belong to two consecutive data blocks $b_1 \neq b_2$, i.e., $b_2 = b_1 - 1$ when $\mu > 0$ and $b_2 = b_1 + 1$ when $\mu < 0$ (the corresponding term in $c_r(t;0)$ is denoted by $\mathfrak{c}_r^{(2)}(t;\tau)$.

1) For $b_1 = b_2$ and with $m_1 = m$ and $m_2 = m_1 - \mu$, $\mu > 0$[5], the corresponding term in the AF in (2.12) is given by

$$\mathfrak{c}_r^{(1)}(t;\tau) = \sum_{b=-\infty}^{\infty} \sum_{m=\mu}^{M-1} \mathrm{E}\left[\tilde{x}_m^b (\tilde{x}_{m-\mu}^b)^*\right] g(t-mT-bMT)g^*(t-mT-bMT). \tag{2.20}$$

[5]The case of $\mu < 0$ will be subsequently discussed.

By splitting the summation in (2.20) over m odd and m even, $\mathfrak{c}_r^{(1)}(t;\tau)$ is further expressed as

$$\begin{aligned}\mathfrak{c}_r^{(1)}(t;\tau) = \quad & \sum_{b=-\infty}^{\infty}\Bigg(\sum_{\substack{m=\mu\\ \text{odd}}}^{M-1}\mathrm{E}\left[\tilde{x}_m^b(\tilde{x}_{m-\mu}^b)^*\right]g(t-mT-bMT)g^*(t-mT-bMT)\\ & +\sum_{\substack{m=\mu+1\\ \text{even}}}^{M-1}\mathrm{E}\left[\tilde{x}_m^b(\tilde{x}_{m-\mu}^b)^*\right]g(t-mT-bMT)g^*(t-mT-bMT)\Bigg),\end{aligned} \tag{2.21}$$

where m =$2n+1$ in the first term and m =$2n$ in the second term, $n=0,...,N-1$. By further writing m as a function of n, (2.21) becomes

$$\begin{aligned}\mathfrak{c}_r^{(1)}(t;\tau) = \quad & \sum_{b=-\infty}^{\infty}\Bigg(\sum_{n=\frac{\mu-1}{2}}^{N-1}\mathrm{E}\left[\tilde{x}_{2n+1}^b(\tilde{x}_{2n+1-\mu}^b)^*\right]g(t-(2n+1)T-bMT)\\ & \times g^*(t-(2n+1)T-bMT)\\ & +\sum_{n=\frac{\mu+1}{2}}^{N-1}\mathrm{E}\left[\tilde{x}_{2n}^b(\tilde{x}_{2n-\mu}^b)^*\right]g(t-2nT-bMT)g^*(t-2nT-bMT)\Bigg).\end{aligned} \tag{2.22}$$

By replacing (2.5) into (2.22), with $Q=2$, one can write

$$\begin{aligned}\mathfrak{c}_r^{(1)}(t;\tau) = \quad & \sum_{b=-\infty}^{\infty}\Bigg(\sum_{n=\frac{\mu-1}{2}}^{N-1}\mathrm{E}\left[\frac{1}{2N}\sum_{p=0}^{N-1}\frac{x_p^b\left(x_{n_1}^b\right)^*}{1-e^{j\pi\left(\frac{2n-2p+1}{N}\right)}}\right]\\ & \times g(t-(2n+1)T-bMT)g^*(t-(2n+1)T-bMT)\\ & +\sum_{n=\frac{\mu+1}{2}}^{N-1}\mathrm{E}\left[\frac{1}{2N}\sum_{p=0}^{N-1}\frac{x_n^b(x_p^b)^*}{1-e^{-j\pi\left(\frac{2n_2-2p+1}{N}\right)}}\right]\\ & \times g(t-2nT-bMT)g^*(t-2nT-bMT)\Bigg).\end{aligned} \tag{2.23}$$

$E[x_p^b(x_{n_1}^b)^*]$ in the first term has non-zero significant values when $p=n_1$. By expressing $\tilde{x}_{2n+1-\mu}^b = x_{n_1}^b$ from the first branch of (2.5), one can also observe that

$2n_1 = 2n + 1 - \mu$. As such, $n - p = \frac{\mu-1}{2}$. On the other hand, $\mathrm{E}[x_n^b (x_p^b)^*]$ in the second term has non-zero significant values when $n = p$. By expressing $\tilde{x}_{2n-\mu}^b = \frac{1}{2N} \sum_{p=0}^{N-1} \frac{x_p^b}{1-e^{j\pi\left(\frac{2n_2-2p+1}{N}\right)}}$ from the second branch of (2.5), one can also observe that $2n - \mu = 2n_2 + 1$. As such, this occurs when $n_2 - p = -\frac{\mu+1}{2}$.

Based on the above discussion, one can re-write (2.23) as

$$\begin{aligned}\mathfrak{c}_r^{(1)}(t;\tau) = \; & \tfrac{c_x}{2N} \tfrac{1}{1-e^{j\pi\frac{\mu}{N}}} \sum_{b=-\infty}^{\infty} \Bigg(\sum_{n=\frac{\mu-1}{2}}^{N-1} g(t-(2n+1)T-bMT) g^*(t-(2n+1)T-bMT) \\ & + \sum_{n=\frac{\mu+1}{2}}^{N-1} g(t-2nT-bMT) g^*(t-2nT-bMT) \Bigg).\end{aligned} \tag{2.24}$$

With $m = 2n+1$ in the first term and $m = 2n$ in the second term, one can re-write (2.24) as

$$\begin{aligned}\mathfrak{c}_r^{(1)}(t;\tau) = \; & \tfrac{c_x}{2N} \tfrac{1}{1-e^{j\pi\frac{\mu}{N}}} \sum_{b=-\infty}^{\infty} \Bigg(\sum_{\substack{m=\mu \\ \text{odd}}}^{M-1} g(t-mT-bMT) g^*(t-mT-bMT) \\ & + \sum_{\substack{m=\mu+1 \\ \text{even}}}^{M-1} g(t-mT-bMT) g^*(t-mT-bMT) \Bigg). \\ = \; & \tfrac{c_x}{2N} \tfrac{1}{1-e^{j\pi\frac{\mu}{N}}} \sum_{b=-\infty}^{\infty} \sum_{m=\mu}^{M-1} g(t-mT-bMT) g^*(t-mT-bMT),\end{aligned} \tag{2.25}$$

and with $k = bM + m$, (2.25) can be further written as

$$\mathfrak{c}_r^{(1)}(t;\tau) = \; \tfrac{c_x}{2N} \tfrac{1}{1-e^{j\pi\frac{\mu}{N}}} \left[g(t) g^*(t) \right] \otimes \sum_{k=-\infty}^{\infty} \delta(t-kT), \tag{2.26}$$

where $\otimes$ denotes the convolutional operator.

By following the above procedure, one can find the expression for $\mathfrak{c}_r^{(1)}(t;\tau)$ for $\mu < 0$ as

$$\mathfrak{c}_r^{(1)}(t;\tau) = \frac{c_x}{2N}\frac{1}{1-e^{-j\pi\frac{\mu}{N}}}\left[g(t)g^*(t)\right] \otimes \sum_{k=-\infty}^{\infty}\delta(t-kT). \tag{2.27}$$

Based on (2.26) and (2.27), one can easily express

$$\mathfrak{c}_r^{(1)}(t;\tau) = \frac{c_x}{2N}\frac{1}{1-e^{j\pi\frac{|\mu|}{N}}}\left[g(t)g^*(t)\right] \otimes \sum_{k=-\infty}^{\infty}\delta(t-kT).$$

2) For $b_1 = b$, $b_2 = b-1$, and with $m_1 = m$ and $m_2 = M-\mu+m$, where $\mu > 0$[5], (2.12) becomes

$$\mathfrak{c}_r^{(2)}(t;\tau) = \sum_{b=-\infty}^{\infty}\sum_{m=0}^{\mu-1}\mathrm{E}\left[\tilde{x}_m^b(\tilde{x}_{M-\mu+m}^{b-1})^*\right] g(t-mT-bMT)g^*(t-mT-bMT).$$

Note that $\mathrm{E}\left[\tilde{x}_m^b(\tilde{x}_{M-\mu+m}^{b-1})^*\right]$ is zero (the symbols belong to different blocks) and there is no contribution of $\mathfrak{c}_r^{(2)}(t;\tau)$ to $c_r(t;\tau)$.

Similarly, one can show that $\mathfrak{c}_r^{(2)}(t;\tau)$ for $b_1 = b$ and $b_2 = b+1$, $\mu < 0$, does not contribute to $c_r(t;\tau)$.

To summarize, for delays $\tau = \mu T$, $\mu = \pm 1, \pm 3, ..., \pm(M-1)$ (odd integer), the AF is expressed as

$$c_r(t;\tau) = \frac{c_x}{2N}\frac{1}{1-e^{j\pi\frac{|\mu|}{N}}}\left[g(t)g^*(t)\right] \otimes \sum_{k=-\infty}^{\infty}\delta(t-kT). \tag{2.28}$$

Case (3): Delay $\tau = \mu T + \tau_s$, $\mu = \pm 2, \pm 4, ..., \pm(M-2)$ (even integer), $\tau_s = 0$

In the following, we derive the analytical expression for the AF at delay $\tau = \mu T$, $\mu = \pm 2, \pm 4, \pm(M-2)$. An example is provided in Fig. 2.6 for $\mu = 2$.

Similarly to case (2), one can easily show that the term in $c_r(t;\tau)$, which corresponds to different data blocks ($b_1 \neq b_2$) in (2.12), is zero. As such, we consider here only the term that corresponds to the same data block.

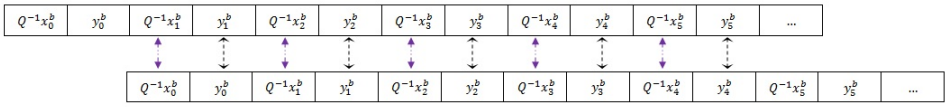

Fig. 2.6: SC-FDMA symbols for $\mu = 2$.

With $b_1 = b_2 = b,\ m_1 = m$, and $m_2 = m_1 - \mu$, $\mu > 0$[5], (2.12) becomes

$$c_r(t;\tau) = \sum_{b=-\infty}^{\infty} \sum_{m=\mu}^{M-1} \mathrm{E}\left[\tilde{x}_m^b (\tilde{x}_{m-\mu}^b)^*\right] g(t - mT - bMT) g^*(t - mT - bMT). \tag{2.29}$$

By splitting the summation in (2.29) over m even and m odd, $c_r(t;\tau)$ becomes

$$\begin{aligned} c_r(t;\tau) = \sum_{b=-\infty}^{\infty} \Bigg(& \sum_{\substack{m=\mu \\ \text{even}}}^{M-1} \mathrm{E}\left[\tilde{x}_m^b (\tilde{x}_{m-\mu}^b)^*\right] g(t - mT - bMT) g^*(t - mT - bMT) \\ & + \sum_{\substack{m=\mu+1 \\ \text{odd}}}^{M-1} \mathrm{E}\left[\tilde{x}_m^b (\tilde{x}_{m-\mu}^b)^*\right] g(t - mT - bMT) g^*(t - mT - bMT) \Bigg), \end{aligned} \tag{2.30}$$

where $m = 2n$ in the first term and $m = 2n + 1$ in the second term, $n = 0, ..., N - 1$. By further writing m as a function of n, (2.30) becomes

$$c_r(t;\tau) = \sum_{b=-\infty}^{\infty}\Bigg(\sum_{n=\frac{\mu}{2}}^{N-1}\mathrm{E}\left[\tilde{x}^b_{2n}(\tilde{x}^b_{2n-\mu})^*\right] g(t-2nT-bMT)g^*(t-2nT-bMT) + \sum_{n=\frac{\mu}{2}}^{N-1}\mathrm{E}\left[\tilde{x}^b_{2n+1}(\tilde{x}^b_{2n+1-\mu})^*\right] g(t-(2n+1)T-bMT)g^*(t-(2n+1)T-bMT)\Bigg), \tag{2.31}$$

and by replacing (2.5) into (2.31), with $Q = 2$ one can write

$$c_r(t;\tau) = \sum_{b=-\infty}^{\infty}\Bigg(\sum_{n=\frac{\mu}{2}}^{N-1}\tfrac{1}{4}\mathrm{E}\left[\, x^b_n(x^b_{n-\frac{\mu}{2}})^*\right] g(t-2nT-bMT)g^*(t-2nT-bMT) + \sum_{n=\frac{\mu}{2}}^{N-1}\mathrm{E}\left[\frac{1}{N^2}\sum_{p_1=0}^{N-1}\sum_{p_2=0}^{N-1}\frac{x^b_{p_1}(x^b_{p_2})^*}{\left(1-e^{\,j\pi\left(\frac{2n-2p_1+1}{N}\right)}\right)\left(1-e^{\,-j\pi\left(\frac{2n'-2p_2+1}{N}\right)}\right)}\right] \times g(t-(2n+1)T-bMT)g^*(t-(2n+1)T-bMT)\Bigg). \tag{2.32}$$

Clearly, $\mathrm{E}\left[\, x^b_n(x^b_{n-\frac{\mu}{2}})^*\right] = 0$ for any $\mu \neq 0$ (independent symbols), and $c_r(t,\tau)$ can be expressed as

$$c_r(t;\tau) = \sum_{b=-\infty}^{\infty}\sum_{n=\frac{\mu}{2}}^{N-1}\mathrm{E}\left[\frac{1}{N^2}\sum_{p_1=0}^{N-1}\sum_{p_2=0}^{N-1}\frac{x^b_{p_1}(x^b_{p_2})^*}{\left(1-e^{\,j\pi\left(\frac{2n-2p_1+1}{N}\right)}\right)\left(1-e^{\,-j\pi\left(\frac{2n'-2p_2+1}{N}\right)}\right)}\right] \times g(t-(2n+1)T-bMT)g^*(t-(2n+1)T-bMT)\Bigg). \tag{2.33}$$

Furthermore, $c_r(t;\tau)$ in (2.33) is non-zero if and only if $p_1 = p_2 = p$. By expressing $\tilde{x}^b_{2n+1-\mu}$ in (2.31) based on (2.5), one can see that $2n' + 1 = 2n + 1 - \mu$. As such, $n' = n - \frac{\mu}{2}$. Based on this observation, (2.33) becomes

$$c_r(t;\tau) = c_x \sum_{b=-\infty}^{\infty} \sum_{n=\frac{\mu}{2}}^{N-1} \left[\frac{1}{N^3} \sum_{p=0}^{N-1} \frac{1}{\left(1-e^{j\pi\left(\frac{2n-2p+1}{N}\right)}\right)\left(1-e^{-j\pi\left(\frac{2n-2p-\mu+1}{N}\right)}\right)} \right] \times g(t-(2n+1)T-bMT)g^*(t-(2n+1)T-bMT). \tag{2.34}$$

By evaluating (2.34) numerically, one obtains that

$$c_r(t,\tau) = 0, \; \forall\, \mu = \pm 2, ..., \pm(M-2). \tag{2.35}$$

Similarly, one can show that (2.35) holds for $\mu < 0$.

Case (4): Delay $\tau = \pm\tau_s$, $0 < \tau_s < T$

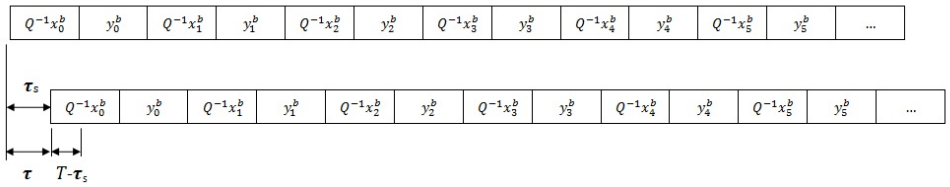

Fig. 2.7: SC-FDMA symbols for $\tau = \tau_s$.

In this case, $c_r(t;\tau)$ is a combination between Cases (1) and (2), i.e.,

$$\begin{aligned} c_r(t;\tau) &= \tfrac{T-\tau_s}{T}\tfrac{c_x}{4}\left[g(t)g^*(t)\right] \otimes \sum_{k=-\infty}^{\infty} \delta(t-kT) + \tfrac{\tau_s}{T}\tfrac{c_x}{2N}\tfrac{1}{1-e^{j\frac{\pi}{N}}}\left[g(t)g^*(t)\right] \otimes \sum_{k=-\infty}^{\infty} \delta(t-kT) \\ &= \left(\tfrac{T-\tau_s}{4T} + \tfrac{\tau_s}{2NT}\tfrac{1}{1-e^{j\frac{\pi}{N}}}\right) c_x \left[g(t)g^*(t)\right] \otimes \sum_{k=-\infty}^{\infty} \delta(t-kT). \end{aligned} \tag{2.36}$$

Case (5): Delay $\tau = \mu T + \mathrm{sgn}(\mu)\tau_s$, $\mu = \pm 1, \pm 3, ..., \pm(M-1)$ (**odd integer**),

$0 < \tau_s < T$, and $\mathrm{sgn}(\mu)$ represents the signum function of a real number μ.

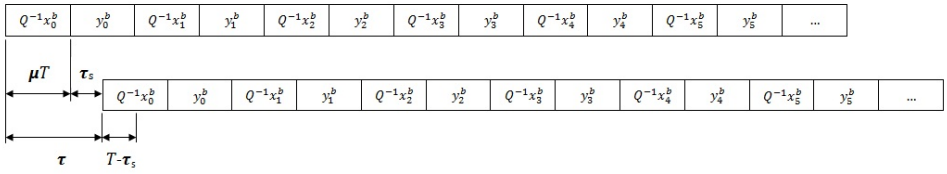

Fig. 2.8: SC-FDMA symbols for $\tau = \mu T + \tau_s$, $\mu = 1$.

Similarly to Cases (2) and (3), one can show that $c_r(t;\tau)$ is as in (2.28) with a weighting factor $\frac{T-\tau_s}{T}$, i.e.,

$$c_r(t;\tau) = \frac{T-\tau_s}{T}\frac{c_x}{2N}\frac{1}{1-e^{j\pi\frac{|\mu|}{N}}}\left[g(t)g^*(t)\right] \otimes \sum_{k=-\infty}^{\infty}\delta(t-kT). \tag{2.37}$$

Note that when $\tau_s = 0$, $c_r(t;\tau)$ is as given in (2.28).

Case (6): Delay $\tau = \mu T + \text{sgn}(\mu)\tau_s$, $\mu = \pm 2, \pm 4, ..., \pm(M-2)$ (**even integer**), $0 < \tau_s < T$

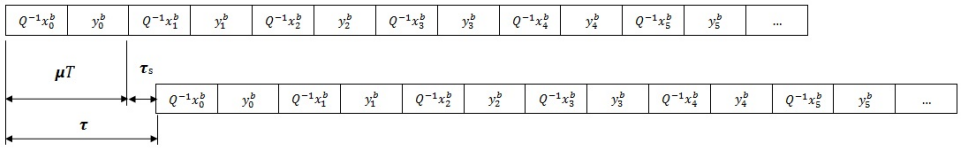

Fig. 2.9: SC-FDMA symbols for $\tau = \mu T + \tau_s$, $\mu = 2$.

Similarly to Cases (2) and (3), one can show that $c_r(t;\tau)$ is the same as (2.28) with weighting factor $\frac{\tau_s}{T}$ and $\mu + 1$ instead of μ, i.e.,

$$c_r(t;\tau) = \frac{\tau_s}{T}\frac{c_x}{2N}\frac{1}{1-e^{j\pi\frac{|\mu+1|}{N}}}\left[g(t)g^*(t)\right] \otimes \sum_{k=-\infty}^{\infty}\delta(t-kT). \tag{2.38}$$

Note that when $\tau_s = 0$, $c_r(t;\tau)$ is as given in (2.35).

Case (7): Delay $\tau = \mu T + \text{sgn}(\mu)\tau_s,\ |\ \mu\ | \geq M$

One can easily show that $c_r(t;\tau)$ is zero, as the symbols belong to different data blocks,

$$c_r(t;\tau) = 0. \tag{2.39}$$

Based on (2.19), (2.28), (2.35), (2.36), (2.37), (2.38), and (2.39), the AF expression can be written as

$$c_r(t;\tau) = \begin{cases} \left(\frac{T-\tau_s}{4T} + \frac{\tau_s}{2NT}\frac{1}{1-e^{j\frac{\pi}{N}}}\right) c_x\left[g(t)g^*(t)\right] \otimes \sum\limits_{k=-\infty}^{\infty} \delta(t-kT), \\ \text{for } \tau = \pm\tau_s,\ 0 \leq \tau_s < T, \\ \frac{T-\tau_s}{T} A(\mu)\left[g(t)g^*(t)\right] \otimes \sum\limits_{k=-\infty}^{\infty} \delta(t-kT), \\ \text{for } \tau = \mu T + \text{sgn}(\mu)\tau_s,\ \mu = \pm 1, \pm 3, \ldots, \pm(M-1),\ 0 \leq \tau_s < T, \\ \frac{\tau_s}{T} A(\mu+1)\left[g(t)g^*(t)\right] \otimes \sum\limits_{k=-\infty}^{\infty} \delta(t-kT), \\ \text{for } \tau = \mu T + \text{sgn}(\mu)\tau_s,\ \mu = \pm 2, \pm 4, \ldots, \pm(M-2),\ 0 \leq \tau_s < T, \\ 0,\ \text{otherwise}, \end{cases} \tag{2.40}$$

where $A(\mu) = \frac{c_x}{2N}\frac{1}{1-e^{j\pi\frac{|\mu|}{N}}}$.

By taking the Fourier transform of (2.40), one can obtain

$$\Im\{c_r(t;\tau)\} = \begin{cases} \left(\frac{T-\tau_s}{4T} + \frac{\tau_s}{2NT}\frac{1}{1-e^{j\frac{\pi}{N}}}\right) c_x T^{-1} \int_{-\infty}^{\infty} g(t)g^*(t)e^{-j2\pi\beta t}dt \sum_{k=-\infty}^{\infty} \delta(\beta - kT^{-1}), \\ \text{for } \tau = \pm\tau_s,\ 0 \le \tau_s < T, \\ \frac{T-\tau_s}{T} A(\mu) T^{-1} \int_{-\infty}^{\infty} g(t)g^*(t)e^{-j2\pi\beta t}dt \sum_{k=-\infty}^{\infty} \delta(\beta - kT^{-1}), \\ \text{for } \tau = \mu T + \text{sgn}(\mu)\tau_s,\ \mu = \pm 1, \pm 3, \ldots, \pm(M-1), 0 \le \tau_s < T, \\ \frac{\tau_s}{T} A(\mu+1) T^{-1} \int_{-\infty}^{\infty} g(t)g^*(t)e^{-j2\pi\beta t}dt \sum_{k=-\infty}^{\infty} \delta(\beta - kT^{-1}), \\ \text{for } \tau = \mu T + \text{sgn}(\mu)\tau_s,\ \mu = \pm 2, \pm 4, \ldots, \pm(M-2), 0 \le \tau_s < T, \\ 0,\ \text{otherwise.} \end{cases} \tag{2.41}$$

From (2.41), one can notice that $\Im\{c_r(t,\tau)\} \neq 0$ if only if $\beta = kT^{-1}$, with k integer. By taking the inverse Fourier transform of (2.41) and using (2.7), one can show that $c_r(\beta;\tau)$ can be expressed as

$$c_r(\beta;\tau) = \begin{cases} \left(\frac{T-\tau_s}{4T} + \frac{\tau_s}{2NT}\frac{1}{1-e^{j\frac{\pi}{N}}}\right) c_x T^{-1} \int_{-\infty}^{\infty} g(t)g^*(t)e^{-j2\pi\beta t}dt, \\ \text{for } \tau = \pm\tau_s,\ \beta = kT^{-1},\ k \text{ integer},\ 0 \le \tau_s < T, \\ \frac{T-\tau_s}{T} A(\mu) T^{-1} \int_{-\infty}^{\infty} \left[g(t)g^*(t)\right] e^{-j2\pi\beta t}dt, \\ \text{for } \tau = \mu T + \text{sgn}(\mu)\tau_s,\ \mu = \pm 1, \pm 3, \ldots, \pm(M-1) \text{ and } \beta = kT^{-1}, \\ k \text{ integer}, 0 \le \tau_s < T, \\ \frac{\tau_s}{T} A(\mu+1) T^{-1} \int_{-\infty}^{\infty} \left[g(t)g^*(t)\right] e^{-j2\pi\beta t}dt, \\ \text{for } \tau = \mu T + \text{sgn}(\mu)\tau_s,\ \mu = \pm 2, \pm 4, \ldots, \pm(M-2) \text{ and } \beta = kT^{-1}, \\ k \text{ integer}, 0 \le \tau_s < T, \\ 0,\ \text{otherwise}. \end{cases} \tag{2.42}$$

The analytical closed-form expression for the CAF and set of CFs for the discrete SC-FDMA signals $r(n) = r(t)|_{t=nf_s}$, $f_s = \rho/T$, with ρ as the oversampling factor, can be written according to (2.9) as

$$c_r(\tilde{\beta};\tilde{\tau}) = \begin{cases} \left(\frac{\rho-\tilde{\tau}_s}{4\rho} + \frac{\tilde{\tau}_s}{2N\rho}\frac{1}{1-e^{j\frac{\pi}{N}}}\right)\rho^{-1}\sum\limits_{n=-\infty}^{\infty} g(n)g^*(n)e^{-j2\pi\tilde{\beta}n},\ 0<\tilde{\tau}_s<\rho, \\ \text{for } \tilde{\tau}=\pm\tilde{\tau}_s, \ \text{ and } \tilde{\beta}=k\rho^{-1},\ k \text{ integer}, \\ \frac{\rho-\tilde{\tau}_s}{\rho}A(\mu)\rho^{-1}\sum\limits_{n=-\infty}^{\infty} g(n)g^*(n)e^{-j2\pi\tilde{\beta}n}, \\ \text{for } \tilde{\tau}=\mu\rho+\text{sgn}(\mu)\tilde{\tau}_s,\ \mu=\pm1,\pm3,\ldots,\pm(M-1) \text{ and } \tilde{\beta}=k\rho^{-1},\ k \text{ integer}, \\ 0\le\tilde{\tau}_s<\rho, \\ \frac{\tilde{\tau}_s}{\rho}A(\mu+1)\rho^{-1}\sum\limits_{n=-\infty}^{\infty} g(n)g^*(n)e^{-j2\pi\tilde{\beta}n}, \\ \text{for } \tilde{\tau}=\mu\rho+\text{sgn}(\mu)\tilde{\tau}_s,,\ \mu=\pm2,\pm4,\ldots,\pm(M-2) \text{ and } \tilde{\beta}=k\rho^{-1},\ k \text{ integer}, \\ 0\le\tilde{\tau}_s<\rho, \\ 0,\ \text{otherwise}, \end{cases} \tag{2.43}$$

where $\tilde{\tau}=\frac{\tau}{T_s}$ and $\tilde{\tau}_s=\frac{\tau_s}{T_s}$, with T_s as the sampling period.

Figs. 2.10 and 2.11 show the magnitude of the theoretical and estimated CAF at zero CF versus positive delays for the SC-FDMA signal in (2.6), respectively. The parameters of the transmitted SC-FDMA signal are: 1.4 MHz double-sided bandwidth, FFT size $N=64$, IFFT size $M=128$, $Q=2$, 16-QAM modulation with unit variance constellation, a root raised cosine pulse shape with a roll-off factor of 0.35 at transmit-side, $\rho=4$, a Butterworth low-pass filter of order 13 used as the receive filter, and observation time 20 ms.

Figs. 2.12 and 2.13 show the magnitude of theoretical and estimated CAF at zero delay versus cycle frequency, respectively. Moreover, Figs. 2.14 and 2.15 show the magnitude of theoretical and estimated CAF at delay ρ versus cycle frequency. As one can notice, simulations results confirm theoretical findings.

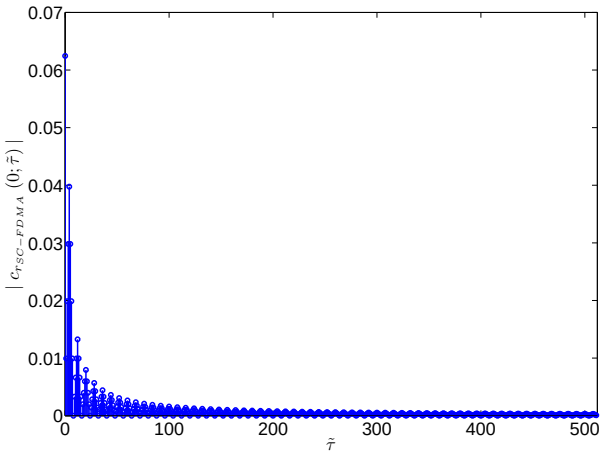

Fig. 2.10: Theoretical results for the CAF magnitude at zero CF ($\tilde{\beta} = 0$) versus positive delays, $\tilde{\tau}$, for SC-FDMA signals.

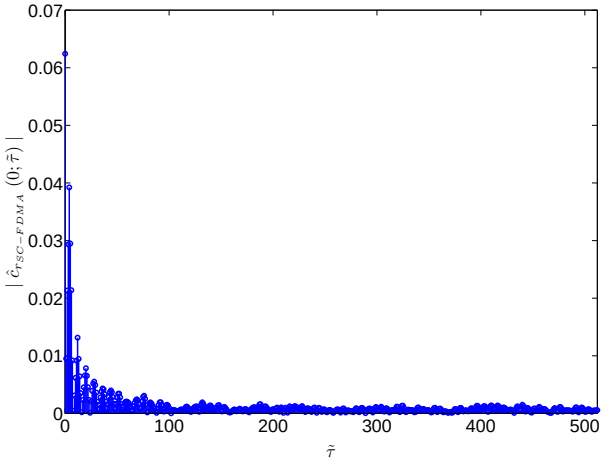

Fig. 2.11: Simulation results for the CAF magnitude at zero CF ($\tilde{\beta} = 0$) versus positive delays, $\tilde{\tau}$, for SC-FDMA signals.

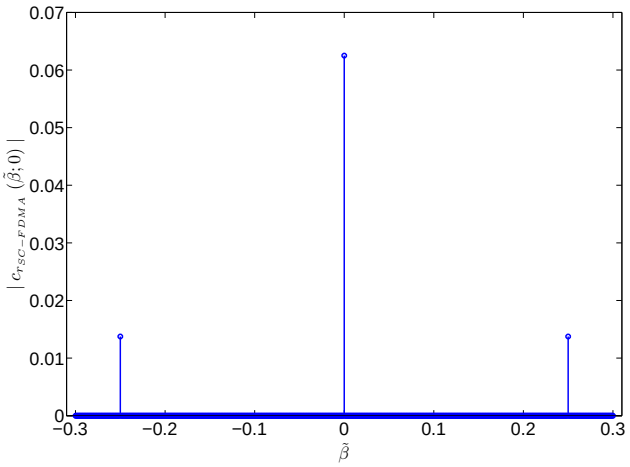

Fig. 2.12: Theoretical results for the CAF magnitude at zero delay ($\tilde{\tau} = 0$) versus cycle frequency, $\tilde{\beta}$, for SC-FDMA signals.

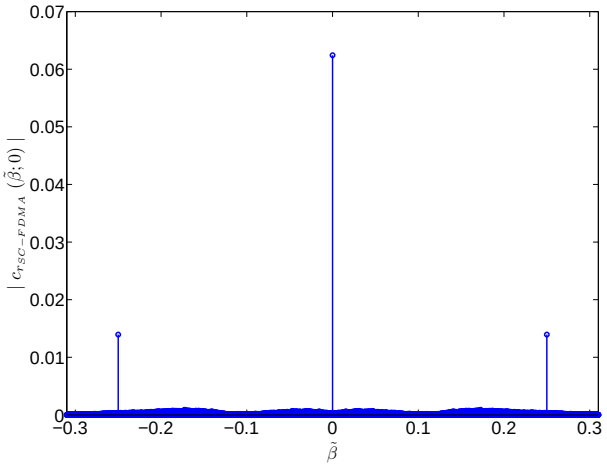

Fig. 2.13: Simulation results for the CAF magnitude at zero delay ($\tilde{\tau} = 0$) versus cycle frequency, $\tilde{\beta}$, for SC-FDMA signals.

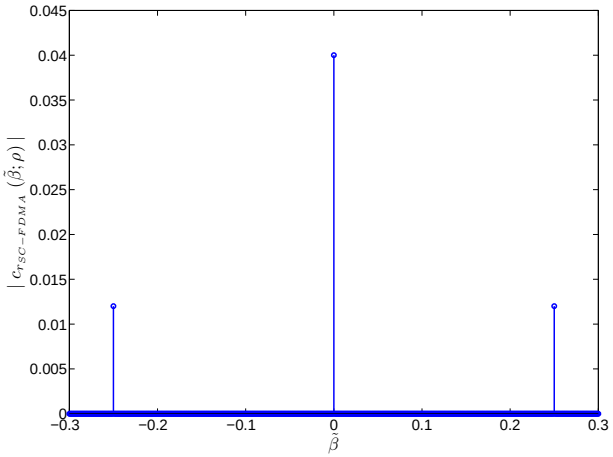

Fig. 2.14: Theoretical results for the CAF magnitude at $\tilde{\tau} = \rho$ versus cycle frequency, $\tilde{\beta}$, for SC-FDMA signals.

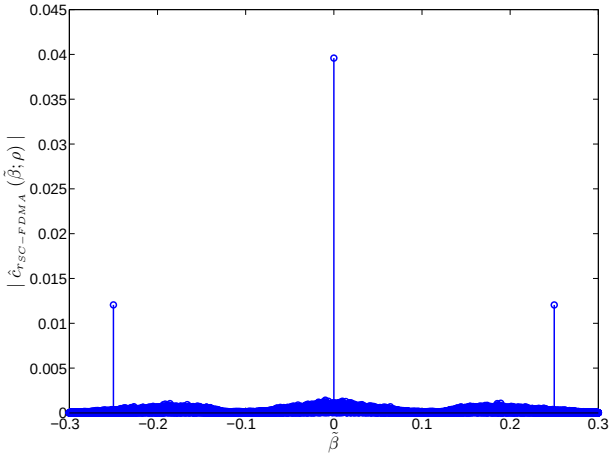

Fig. 2.15: Simulation results for the CAF magnitude at $\tilde{\tau} = \rho$ versus cycle frequency, $\tilde{\beta}$, for SC-FDMA signals.

2.5 CAF and Set of CFs for the SC-FDMA with CP

To combat the inter-symbol interference caused by the channel delay spread in the SC-FDMA transmission, a cyclic prefix (CP) of L symbols is added at the beginning of every M information symbols ($L< M$) for each block. According to the standard signals [24–26], L is assumed a multiple integer of Q. The structure of an SC-FDMA block with CP is presented in Fig. 2.16.

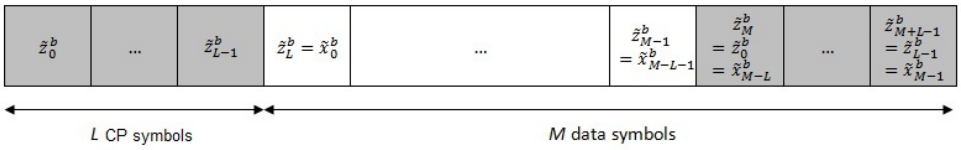

Fig. 2.16: SC-FDMA transmission block.

The received noise-free SC-FDMA signal can be expressed as

$$r_{\text{SC-FDMA}}(t) = \sum_{b=-\infty}^{\infty} \left[\sum_{u=0}^{M+L-1} \tilde{z}_u^b g(t - uT - b(M+L)T) \right], \tag{2.44}$$

where u is the symbol index within a block and $\tilde{z}_u^b$ is the symbol transmitted within the u-th symbol period of block b.

The symbols $\tilde{z}_u^b$ are expressed as

$$\tilde{z}_u^b = \begin{cases} \tilde{x}_{M-L+u}^b, & 0 \le u \le L-1, \\ \\ \tilde{x}_{u-L}^b, & L \le u \le M+L-1. \end{cases} \tag{2.45}$$

Furthermore, with (2.11) and (2.44), the AF of the SC-FDMA signal with CP can

be expressed as

$$\begin{aligned} c_r(t,\tau) &= \sum_{b_1=-\infty}^{\infty}\sum_{b_2=-\infty}^{\infty}\sum_{u_1=0}^{M+L-1}\sum_{u_2=0}^{M+L-1} \mathrm{E}\left[\tilde{z}_{u_1}^{b_1}(\tilde{z}_{u_2}^{b_2})^*\right] g(t-u_1T-b_1(M+L)T) \\ &\quad g^*(t-u_2T-b_2(M+L)T-\tau). \end{aligned} \tag{2.46}$$

The AF of SC-FDMA is investigated in the following cases:

Case (1): Zero delay$(\tau = 0)$

By following the same steps as in Section 3.3, one can show that[4]

$$c_r(t,0) = \frac{c_x}{4}\sum_{b=-\infty}^{\infty}\sum_{u=0}^{M+L-1} g(t-uT-b(M+L)T)g^*(t-uT-b(M+L)T). \tag{2.47}$$

With $k = b(M+L)+u$ in (2.9), one can write

$$c_r(t,0) = \frac{c_x}{4}\left[g(t)g^*(t)\right] \otimes \sum_{k=-\infty}^{\infty}\delta(t-kT). \tag{2.48}$$

Case (2): Delay $\tau = \mu T + \tau_s$, $\mu = \pm 1, \pm 3, ..., \pm(M-L-1)$ **(odd integer)**, $\tau_s = 0$

In the following, we derive the analytical expression for the AF at delay $\tau = \mu T$, $\mu = \pm 1, \pm 3, ..., \pm(M-L-1)$. An example of this case is provided in Fig. 2.17.

Along the same line as in Section 3.3, one can easily show that the terms in $c_r(t,\tau)$ which correspond to different data blocks ($b_1 \neq b_2$) are zero. As such, we consider here the contribution of the terms corresponding to the same data block.

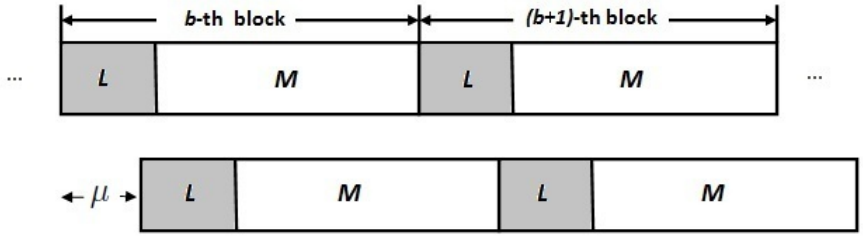

Fig. 2.17: SC-FDMA symbols for $1 \leq \mu \leq M - L - 1$.

In such a case, with $b_1 = b_2 = b$, $u_1 = u$, and $u_2 = u_1 - \mu$, $\mu > 0$[5], (2.46) becomes

$$c_r(t;\tau) = \sum_{b=-\infty}^{\infty} \sum_{u=\mu}^{M+L-1} \mathrm{E}\left[\tilde{z}_u^b \left(\tilde{z}_{u-\mu}^b\right)^*\right] g(t - uT - b(L+M)T) g^*(t - uT - b(L+M)T). \tag{2.49}$$

Furthermore, by emphasizing the possible summation over the CP symbols, (2.49) becomes

$$\begin{aligned} c_r(t;\tau) = \sum_{b=-\infty}^{\infty} \Bigg(& \sum_{u=\mu}^{L-1} \mathrm{E}\left[\tilde{z}_u^b \left(\tilde{z}_{u-\mu}^b\right)^*\right] g(t - uT - b(L+M)T) g^*(t - uT - b(L+M)T) \\ & + \sum_{u=L}^{M+L-1} \mathrm{E}\left[\tilde{z}_u^b \left(\tilde{z}_{u-\mu}^b\right)^*\right] g(t - uT - b(L+M)T) g^*(t - uT - b(L+M)T) \Bigg), \end{aligned} \tag{2.50}$$

and by considering u odd and u even, (2.50) is further expressed as

$$\begin{aligned} c_r(t;\tau) = & \overbrace{\sum_{b=-\infty}^{\infty} \Bigg(\sum_{\substack{u=\mu \\ \text{odd}}}^{L-1} \mathrm{E}\left[\tilde{z}_u^b \left(\tilde{z}_{u-\mu}^b\right)^*\right] g(t - uT - b(L+M)T) g^*(t - uT - b(L+M)T) \Bigg)}^{\mathfrak{c}_r^{(1)}(t;\tau)} \\ & + \overbrace{\sum_{b=-\infty}^{\infty} \Bigg(\sum_{\substack{u=\mu+1 \\ \text{even}}}^{L-1} \mathrm{E}\left[\tilde{z}_u^b \left(\tilde{z}_{u-\mu}^b\right)^*\right] g(t - uT - b(L+M)T) g^*(t - uT - b(L+M)T) \Bigg)}^{\mathfrak{c}_r^{(2)}(t;\tau)} \end{aligned}$$

$$\overbrace{+\sum_{b=-\infty}^{\infty}\Bigg(\sum_{\substack{u=L+1\\ \text{odd}}}^{M+L-1}\mathrm{E}\left[\tilde{z}_u^b\left(\tilde{z}_{u-\mu}^b\right)^*\right]g(t-uT-b(L+M)T)g^*(t-uT-b(L+M)T)\Bigg)}^{\mathfrak{c}_r^{(3)}(t;\tau)}$$
$$\overbrace{+\sum_{b=-\infty}^{\infty}\Bigg(\sum_{\substack{u=L\\ \text{even}}}^{M+L-1}\mathrm{E}\left[\tilde{z}_u^b\left(\tilde{z}_{u-\mu}^b\right)^*\right]g(t-uT-b(L+M)T)g^*(t-uT-b(L+M)T)\Bigg)}^{\mathfrak{c}_r^{(4)}(t;\tau)}. \tag{2.51}$$

With $m = M - L + u$ and by using (2.45), $\mathfrak{c}_r^{(1)}(t;\tau)$ becomes

$$\begin{aligned}\mathfrak{c}_r^{(1)}(t;\tau) = \sum_{b=-\infty}^{\infty}\Bigg(&\sum_{\substack{m=M-L+\mu\\ \text{odd}}}^{M-1}\mathrm{E}\left[\tilde{x}_m^b\left(\tilde{x}_{m-\mu}^b\right)^*\right]g(t-(m-M+L)T-b(L+M)T)\\ &\times g^*(t-(m-M+L)T-b(L+M)T)\Bigg),\end{aligned}$$

and by following the same steps as in Section 3.3, one can show that

$$\begin{aligned}\mathfrak{c}_r^{(1)}(t;\tau) = \frac{c_x}{2N}\frac{1}{1-e^{j\pi\frac{\mu}{N}}}\sum_{b=-\infty}^{\infty}\Bigg(&\sum_{\substack{m=M-L+\mu\\ \text{odd}}}^{M-1}g(t-(m-M+L)T-b(L+M)T)\\ &\times g^*(t-(m-M+L)T-b(L+M)T)\Bigg).\end{aligned} \tag{2.52}$$

Furthermore, by following the same steps as for $\mathfrak{c}_r^{(1)}(t;\tau)$, $\mathfrak{c}_r^{(2)}(t;\tau)$ becomes

$$\begin{aligned}\mathfrak{c}_r^{(2)}(t;\tau) = \frac{c_x}{2N}\frac{1}{1-e^{j\pi\frac{\mu}{N}}}\sum_{b=-\infty}^{\infty}\Bigg(&\sum_{\substack{m=M-L+\mu+1\\ \text{even}}}^{M-1}g(t-(m-M+L)T-b(L+M)T)\\ &\times g^*(t-(m-M+L)T-b(L+M)T)\Bigg).\end{aligned} \tag{2.53}$$

With $m = u - L$ and using (2.45), $\mathfrak{c}_r^{(3)}(t;\tau)$ becomes

$$\begin{aligned}\mathfrak{c}_r^{(3)}(t;\tau) = \quad & \sum_{b=-\infty}^{\infty}\Bigg(\sum_{\substack{m=1\\ \text{odd}}}^{M-1}\mathrm{E}\left[\tilde{x}_m^b\left(\tilde{x}_{m-\mu}^b\right)^*\right] g(t-(m+L)T-b(L+M)T) \\ & \times g^*(t-(m+L)T-b(L+M)T)\Bigg),\end{aligned} \tag{2.54}$$

and by following the same steps as in Section 3.3, one can show that

$$\begin{aligned}\mathfrak{c}_r^{(3)}(t;\tau) = \quad & \tfrac{c_x}{2N}\tfrac{1}{1-e^{j\pi\frac{\mu}{N}}}\sum_{b=-\infty}^{\infty}\Bigg(\sum_{\substack{m=1\\ \text{odd}}}^{M-1} g(t-(m+L)T-b(L+M)T) \\ & \times g^*(t-(m+L)T-b(L+M)T)\Bigg).\end{aligned} \tag{2.55}$$

Furthermore, by following the same steps as in $\mathfrak{c}_r^{(3)}(t;\tau)$, $\mathfrak{c}_r^{(4)}(t;\tau)$ becomes

$$\begin{aligned}\mathfrak{c}_r^{(4)}(t;\tau) = \quad & \tfrac{c_x}{2N}\tfrac{1}{1-e^{j\pi\frac{\mu}{N}}}\sum_{b=-\infty}^{\infty}\Bigg(\sum_{\substack{m=0\\ \text{even}}}^{M-1} g(t-(m+L)T-b(L+M)T) \\ & \times g^*(t-(m+L)T-b(L+M)T)\Bigg).\end{aligned} \tag{2.56}$$

Finally, by substituting (2.52), (2.53), (2.55), and (2.56) in (2.51), and using $u = m - M + L$ in the the expressions of $\mathfrak{c}_r^{(1)}(t;\tau)$ and $\mathfrak{c}_r^{(2)}(t;\tau)$ and $u = m + L$ in the expressions of $\mathfrak{c}_r^{(3)}(t;\tau)$ and $\mathfrak{c}_r^{(4)}(t;\tau)$, (2.51) becomes

$$c_r(t;\tau) = \quad \tfrac{c_x}{2N}\tfrac{1}{1-e^{j\pi\frac{\mu}{N}}}\sum_{b=-\infty}^{\infty}\Bigg(\sum_{u=\mu}^{M+L-1} g(t-uT-b(L+M)T)g^*(t-uT-b(L+M)T)\Bigg). \tag{2.57}$$

Note that $c_r(t;\tau)$ for $\mu < 0$ can be solved by following the above procedure, and it can be shown to be expressed as

$$c_r(t;\tau) = \frac{c_x}{2N}\frac{1}{1-e^{-j\pi\frac{\mu}{N}}}\sum_{b=-\infty}^{\infty}\left(\sum_{u=0}^{M+L-1} g(t-uT-b(L+M)T)g^*(t-uT-b(L+M)T)\right), \tag{2.58}$$

and with $k = b(L+M)+u$, $c_r(t;\tau)$ can be further written as

$$c_r(t;\tau) = \frac{c_x}{2N}\frac{1}{1-e^{j\pi\frac{|\mu|}{N}}}\left[g(t)g^*(t)\right] \otimes \sum_{k=-\infty}^{\infty}\delta(t-kT). \tag{2.59}$$

Case (3): Delay $\tau = \mu T + \tau_s$, $\mu = \pm 2, \pm 4, ..., \pm(M-L)$ **(even integer)**, $\tau_s = 0$

By following the same procedure as in Case (3) of Section 3.3, one can show that AF equals zero, i.e.,

$$c_r(t;\tau) = 0. \tag{2.60}$$

Case (4): Delay $\tau = \pm\tau_s, 0 \le \tau_s < T$

By following Case (4) of Section 3.3, one can show that $c_r(t;\tau)$

$$c_r(t;\tau) = \left(\frac{T-\tau_s}{4T} + \frac{\tau_s}{2NT}\frac{1}{1-e^{j\frac{\pi}{N}}}\right) c_x\left[g(t)g^*(t)\right] \otimes \sum_{k=-\infty}^{\infty}\delta(t-kT) \tag{2.61}$$

Case (5): Delay $\tau = \mu T + \mathrm{sgn}(\mu)\tau_s$, $\mu = \pm 1, \pm 3, ..., \pm(M-L-1)$ **(odd integer)**, $0 < \tau_s < T$

By following Case (5) of Section 3.3, one can show that $c_r(t;\tau)$ is as in (2.59), with a weighting factor of $\frac{T-\tau_s}{T}$, i.e.,

$$c_r(t;\tau) = \frac{T-\tau_s}{T}\quad\frac{c_x}{2N}\frac{1}{1-e^{j\pi\frac{|\mu|}{N}}}\left[g(t)g^*(t)\right] \otimes \sum_{k=-\infty}^{\infty}\delta(t-kT). \tag{2.62}$$

Case (6): Delay $\tau = \mu T + \text{sgn}(\mu)\tau_s,\ \mu = \pm 2, \pm 4, ..., \pm(M-L)$ **(even integer)**, $0 < \tau_s < T$

By following Case (6) of Section 3.3, one can show that $c_r(t;\tau)$ is as in (2.59), with a weighting factor of $\frac{\tau_s}{T}$ and μ replaced by $\mu + 1$, i.e.,

$$c_r(t;\tau) = \frac{\tau_s}{T}\frac{c_x}{2N}\frac{1}{1-e^{j\pi\frac{|\mu+1|}{N}}}\left[g(t)g^*(t)\right] \otimes \sum_{k=-\infty}^{\infty}\delta(t-kT). \tag{2.63}$$

Case (7): Delay $\tau = \mu T + \tau_s,\ \mu = \pm(M-L+1), ..., \pm(M+L-1)$ **(odd and even integers),** $0 \le \tau_s < T$

In the following, we derive the analytical expression for the AF at delay $\tau = \mu T + \tau_s,\ \mu = \pm(M-L), ..., \pm(M+L-1)$.

The analytical expression for the AF at delay $\tau = \mu T + \tau_s,\ \mu = \pm(M-L+1), ..., \pm(M+L-1)$ can be expressed as

a) Delay $\tau = \pm MT + \tau_s,\ \tau_s = 0$

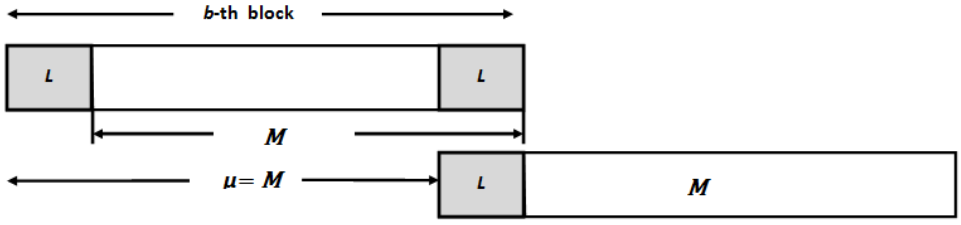

Fig. 2.18: SC-FDMA symbols for $\mu = M$.

By following the same procedure as in Case (1) with block length of L, $c_r(t,\tau)$ can be expressed as

$$\begin{aligned} c_r(t,\tau) &= \sum_{b=-\infty}^{\infty}\sum_{u=0}^{L-1}\frac{c_x}{4}\left[g(t-uT-b(M+L)T)g^*(t-uT-b(M+L)T)\right] \\ &= \frac{c_x}{4}\sum_{u=0}^{L-1}\left[g(t-uT)g^*(t-uT)\right] \otimes \sum_{b=-\infty}^{\infty}\delta(t-b(M+L)T). \end{aligned} \tag{2.64}$$

b) Delay $\tau = \mu T + \text{sgn}(\mu)\tau_s,\ \mu = \pm M,\ 0 < \tau_s < T$

By following the same procedure as in Cases (4)

$$c_r(t,\tau) \ = \left(\frac{T-\tau_s}{4T} + \frac{\tau_s}{2NT}\frac{1}{1-e^{j\frac{\pi}{N}}}\right) c_x \sum_{u=0}^{L-1} [g(t)g^*(t)] \otimes \sum_{k=-\infty}^{\infty} \delta(t-kT) \tag{2.65}$$

c) Delay $\tau = \mu T + \text{sgn}(\mu)\tau_s,\ \mu = \pm(M-L+1), \pm(M-L+3), ..., \pm(M+L-1)$ (odd integer), $0 \le \tau_s < T$

By following the same procedure as in Cases (2) and (5), $c_r(t,\tau)$ can be expressed as

$$\begin{aligned} c_r(t,\tau) \ &= \frac{T-\tau_s}{T}\frac{c_x}{2N}\frac{1}{1-e^{j\pi\frac{|\mu|}{N}}} \sum_{b=-\infty}^{\infty}\sum_{u=0}^{L-1} [g(t-uT-b(M+L)T)g^*(t-uT-b(M+L)T)] \\ &= \frac{T-\tau_s}{T}\frac{c_x}{2N}\frac{1}{1-e^{j\pi\frac{|\mu|}{N}}} \sum_{u=0}^{L-1} [g(t-uT)g^*(t-uT)] \otimes \sum_{b=-\infty}^{\infty} \delta(t-b(M+L)T). \end{aligned} \tag{2.66}$$

d) Delay $\tau = \mu T + \text{sgn}(\mu)\tau_s,\ \mu = \pm(M-L) \pm (M-L+2), \pm(M-2), \pm(M+2),$ $..., \pm(M+L-2)$ (even integer), $0 \le \tau_s < T$

By following the same procedure as in Cases (3) and (6), $c_r(t,\tau)$ can be expressed as

$$c_r(t;\tau) = \ \frac{\tau_s}{T}\frac{c_x}{2N}\frac{1}{1-e^{j\pi\frac{|\mu+1|}{N}}} \sum_{u=0}^{L-1} [g(t-uT)g^*(t-uT)] \otimes \sum_{k=-\infty}^{\infty} \delta(t-b(M+L)T). \tag{2.67}$$

Case (8): Delay $\tau = \mu T + \text{sgn}(\mu)\tau_s,\ \mid \mu \mid \ge M + L$

One can easily see that $c_r(t,\tau)$ for such a case is zero (different data blocks),

$$c_r(t;\tau) = 0. \tag{2.68}$$

Based on (2.48), (2.59), (2.60), (2.61), (2.62), (2.64), (2.65), (2.66), (2.67), and (2.68), the closed-form of the AF of SC-FDMA signal can be expressed as

$$c_r(t;\tau) = \begin{cases} \left(\frac{T-\tau_s}{4T} + \frac{\tau_s}{2NT}\frac{1}{1-e^{j\frac{\pi}{N}}}\right) c_x \left[g(t)g^*(t)\right] \otimes \sum\limits_{k=-\infty}^{\infty} \delta(t-kT), \\ \text{for } \tau = \pm\tau_s,\ 0 \le \tau_s < T \\ \frac{T-\tau_s}{T} A(\mu) \left[g(t)g^*(t)\right] \otimes \sum\limits_{k=-\infty}^{\infty} \delta(t-kT), \\ \text{for } \tau = \mu T + \text{sgn}(\mu)\tau_s,\ \mu = \pm 1, \pm 3, \ldots, \pm(M-L-1),\ 0 \le \tau_s < T, \\ \frac{\tau_s}{T} A(\mu+1) \left[g(t)g^*(t)\right] \otimes \sum\limits_{k=-\infty}^{\infty} \delta(t-kT). \\ \text{for } \tau = \mu T + \text{sgn}(\mu)\tau_s,\ \mu = \pm 2, \pm 4, \ldots, \pm(M-L),\ 0 \le \tau_s < T, \\ \left(\frac{T-\tau_s}{4T} + \frac{\tau_s}{2NT}\frac{1}{1-e^{j\frac{\pi}{N}}}\right) c_x \sum\limits_{u=0}^{L-1} \left[g(t-uT)g^*(t-uT)\right] \otimes \sum\limits_{k=-\infty}^{\infty} \delta(t-b(M+L)T), \\ \text{for } \tau = \mu T + \text{sgn}(\mu)\tau_s,\ \mu = \pm M,\ 0 \le \tau_s < T \\ \frac{T-\tau_s}{T} A(\mu) \sum\limits_{u=0}^{L-1} \left[g(t-uT)g^*(t-uT)\right] \otimes \sum\limits_{b=-\infty}^{\infty} \delta(t-b(M+L)T), \\ \text{for } \tau = \mu T + \text{sgn}(\mu)\tau_s,\ \mu = \pm(M-L+1), \pm(M-L+3), \\ \ldots, \pm(M+L-1), 0 \le \tau_s < T, \\ \frac{\tau_s}{T} A(\mu+1) \sum\limits_{u=0}^{L-1} \left[g(t-uT)g^*(t-uT)\right] \otimes \sum\limits_{b=-\infty}^{\infty} \delta(t-b(M+L)T), \\ \text{for } \tau = \mu T + \text{sgn}(\mu)\tau_s,\ \mu = \pm(M-L+2), \ldots, \pm(M-2), \pm(M+2), \\ \ldots, \pm(M+L-2),\ 0 \le \tau_s < T, \\ 0,\ \text{otherwise}, \end{cases} \tag{2.69}$$

where $A(\mu) = \frac{c_x}{2N}\frac{1}{1-e^{j\pi\frac{|\mu|}{N}}}$.

By taking the Fourier transform of (2.69), one can show that

$$\Im\{c_r(t;\tau)\} = \begin{cases} \left(\frac{T-\tau_s}{4T} + \frac{\tau_s}{2NT}\frac{1}{1-e^{j\frac{\pi}{N}}}\right)c_x T^{-1}\int_{-\infty}^{\infty}[g(t)g^*(t)]\,e^{-j2\pi\beta t}dt\sum_{b=-\infty}^{\infty}\delta(\beta-kT^{-1}), \\ \text{for } \tau = \pm\tau_s,\ 0 \le \tau_s < T \\ \frac{T-\tau_s}{T}A(\mu)T^{-1}\int_{-\infty}^{\infty}[g(t)g^*(t)]\,e^{-j2\pi\beta t}dt\sum_{b=-\infty}^{\infty}\delta(\beta-kT^{-1}), \\ \text{for } \tau = \mu T + \text{sgn}(\mu)\tau_s,\ \mu = \pm1, \pm3, ..., \pm(M-L-1),\ 0 \le \tau_s < T, \\ \frac{\tau_s}{T}A(\mu+1)T^{-1}\int_{-\infty}^{\infty}[g(t)g^*(t)]\,e^{-j2\pi\beta t}dt \times \sum_{b=-\infty}^{\infty}\delta(\beta-kT^{-1}), \\ \text{for } \tau = \mu T + \text{sgn}(\mu)\tau_s,\ \mu = \pm2, \pm4, ..., \pm(M-L),\ 0 \le \tau_s < T, \\ \left(\frac{T-\tau_s}{4T} + \frac{\tau_s}{2NT}\frac{1}{1-e^{j\frac{\pi}{N}}}\right)c_x\left[(M+L)T\right]^{-1}\int_{-\infty}^{\infty}\sum_{u=0}^{L-1}[g(t-uT)g^*(t-uT)]\,e^{-j2\pi\beta t}dt \\ \times\sum_{b=-\infty}^{\infty}\delta(\beta-[b(M+L)T]^{-1}), \\ \text{for } \tau = \mu T + \text{sgn}(\mu)\tau_s,\ \mu = \pm M,\ 0 < \tau_s < T \\ \frac{T-\tau_s}{T}A(\mu)\left[(M+L)T\right]^{-1}\int_{-\infty}^{\infty}\sum_{u=0}^{L-1}[g(t-uT)g^*(t-uT)]\,e^{-j2\pi\beta t}dt \\ \times\sum_{b=-\infty}^{\infty}\delta(\beta-[b(M+L)T]^{-1}), \\ \text{for } \tau = \mu T + \text{sgn}(\mu)\tau_s,\ \mu = \pm(M-L+1), \pm(M-L+3), ..., \pm(M+L-1), \\ 0 \le \tau_s < T, \\ \frac{\tau_s}{T}A(\mu+1)\left[(M+L)T\right]^{-1}\int_{-\infty}^{\infty}\sum_{u=0}^{L-1}[g(t-uT)g^*(t-uT)]\,e^{-j2\pi\beta t}dt \\ \times\sum_{b=-\infty}^{\infty}\delta(\beta-[b(M+L)T]^{-1}), \\ \text{for } \tau = \mu T + \text{sgn}(\mu)\tau_s,\ \mu = \pm(M-L+2), \ldots, \pm(M-2), \pm(M+2), \ldots, \\ \pm(M+L-2),\ 0 \le \tau_s < T, \\ 0,\ \text{otherwise.} \end{cases} \tag{2.70}$$

By taking the inverse Fourier transform of (2.70) and using (2.7), one can show

that $c_r(\beta;\tau)$ can be expressed as

$$c_r(\beta;\tau) = \begin{cases} \left(\frac{T-\tau_s}{4T} + \frac{\tau_s}{2NT}\frac{1}{1-e^{j\frac{\pi}{N}}}\right) c_x T^{-1} \int_{-\infty}^{\infty} [g(t)g^*(t)]\, e^{-j2\pi\beta t} dt, \\ \text{for } \tau = \pm\tau_s,\ 0 \le \tau_s < T, \text{ and } \beta = kT^{-1},\ k \text{ integer}, \\ \frac{T-\tau_s}{T} A(\mu) T^{-1} \int_{-\infty}^{\infty} [g(t)g^*(t)]\, e^{-j2\pi\beta t} dt, \\ \text{for } \tau = \mu T + \text{sgn}(\mu)\tau_s, \text{ where } \mu = \pm 1, \pm 3, \ldots, \pm(M-L-1),\ 0 \le \tau_s < T, \\ \text{and } \beta = kT^{-1},\ k \text{ integer}, \\ \frac{\tau_s}{T} A(\mu+1) T^{-1} \int_{-\infty}^{\infty} [g(t)g^*(t)]\, e^{-j2\pi\beta t} dt, \\ \text{for } \tau = \mu T + \text{sgn}(\mu)\tau_s, \text{ where } \mu = \pm 2, \pm 4, \ldots, \pm(M-L),\ 0 \le \tau_s < T, \\ \text{and } \beta = kT^{-1},\ k \text{ integer}, \\ \left(\frac{T-\tau_s}{4T} + \frac{\tau_s}{2NT}\frac{1}{1-e^{j\frac{\pi}{N}}}\right) c_x \left[(M+L)T\right]^{-1} \int_{-\infty}^{\infty} \sum_{u=0}^{L-1} [g(t-uT)g^*(t-uT)]\, e^{-j2\pi\beta t} dt, \\ \text{for } \tau = \mu T + \text{sgn}(\mu)\tau_s,\ \mu = \pm M,\ 0 \le \tau_s < T, \text{ and } \beta = b[(M+L)T]^{-1},\ b \text{ integer}, \\ \frac{T-\tau_s}{T} A(\mu) \left[(M+L)T\right]^{-1} \int_{-\infty}^{\infty} \sum_{u=0}^{L-1} [g(t-uT)g^*(t-uT)]\, e^{-j2\pi\beta t} dt, \\ \text{for } \tau = \mu T + \text{sgn}(\mu)\tau_s,\ \mu = \pm(M-L+1), \pm(M-L+3), \ldots, \pm(M+L-1), \\ 0 \le \tau_s < T, \text{ and } \beta = b[(M+L)T]^{-1},\ b \text{ integer}, \\ \frac{\tau_s}{T} A(\mu+1) \left[(M+L)T\right]^{-1} \int_{-\infty}^{\infty} \sum_{u=0}^{L-1} [g(t-uT)g^*(t-uT)]\, e^{-j2\pi\beta t} dt, \\ \text{for } \tau = \mu T + \text{sgn}(\mu)\tau_s,\ \mu = \pm(M-L+2), \ldots, \pm(M-2), \pm(M+2), \ldots, \\ \pm(M+L-2),\ 0 \le \tau_s < T, \text{ and } \beta = b[(M+L)T]^{-1},\ b \text{ integer}, \\ 0, \text{ otherwise.} \end{cases} \tag{2.71}$$

The analytical closed-form expression for the CAF and set of CFs for the discrete SC-FDMA signals $r(n) = r(t)|_{t=nf_s}$, $f_s = \rho/T$, with ρ as the oversampling factor, can be written according to (2.10) as

$$c_r(\tilde{\beta};\tilde{\tau}) = \begin{cases} \left(\frac{\rho-\tilde{\tau}_s}{4\rho} + \frac{\tilde{\tau}_s}{2N\rho}\frac{1}{1-e^{j\frac{\pi}{N}}}\right) c_x \rho^{-1} \sum\limits_{n=-\infty}^{\infty} [g(n)g^*(n)]\, e^{-j2\pi\tilde{\beta}n}, \\ \text{for } \tilde{\tau} = \pm\tilde{\tau}_s,\ 0 \le \tilde{\tau}_s < \rho, \text{ and } \tilde{\beta} = k\rho^{-1},\ k \text{ integer}, \\ \frac{\rho-\tilde{\tau}_s}{\rho} A(\mu)\rho^{-1} \sum\limits_{n=-\infty}^{\infty} [g(n)g^*(n)]\, e^{-j2\pi\tilde{\beta}n}, \\ \text{for } \tilde{\tau} = \mu\rho + \text{sgn}(\mu)\tilde{\tau}_s, \text{ where } \mu = \pm 1, \pm 3, \ldots, \pm(M-L-1),\ 0 \le \tilde{\tau}_s < \rho, \\ \text{and } \tilde{\beta} = k\rho^{-1},\ k \text{ integer}, \\ \frac{\tilde{\tau}_s}{\rho} A(\mu+1)\rho^{-1} \sum\limits_{n=-\infty}^{\infty} [g(n)g^*(n)]\, e^{-j2\pi\tilde{\beta}n}, \\ \text{for } \tilde{\tau} = \mu\rho + \text{sgn}(\mu)\tilde{\tau}_s, \text{ where } \mu = \pm 2, \pm 4, \ldots, \pm(M-L),\ 0 \le \tilde{\tau}_s < \rho, \\ \text{and } \tilde{\beta} = k\rho^{-1},\ k \text{ integer}, \\ \left(\frac{\rho-\tilde{\tau}_s}{4\rho} + \frac{\tilde{\tau}_s}{2N\rho}\frac{1}{1-e^{\pm j\frac{\pi}{N}}}\right) c_x \left[(M+L)\rho\right]^{-1} \sum\limits_{u=0}^{L-1}\sum\limits_{n=-\infty}^{\infty} [g(n-u\rho)g^*(n-u\rho)]\, e^{-j2\pi\tilde{\beta}n}, \\ \text{for } \tilde{\tau} = \mu\rho + \text{sgn}(\mu)\tilde{\tau}_s,\ \mu = \pm M,\ 0 \le \tilde{\tau}_s < \rho, \text{ and } \tilde{\beta} = b[(M+L)\rho]^{-1},\ b \text{ integer}, \\ \frac{\rho-\tilde{\tau}_s}{\rho} A(\mu) \left[(M+L)\rho\right]^{-1} \sum\limits_{u=0}^{L-1}\sum\limits_{n=-\infty}^{\infty} [g(n-u\rho)g^*(n-u\rho)]\, e^{-j2\pi\tilde{\beta}n}, \\ \text{for } \tilde{\tau} = \mu\rho + \text{sgn}(\mu)\tilde{\tau}_s,\ \mu = \pm(M-L+1), \pm(M-L+3), \ldots, \pm(M+L-1), \\ 0 \le \tilde{\tau}_s < \rho, \text{ and } \tilde{\beta} = b[(M+L)\rho]^{-1},\ b \text{ integer}, \\ \frac{\tilde{\tau}_s}{\rho} A(\mu+1) \left[(M+L)\rho\right]^{-1} \sum\limits_{u=0}^{L-1}\sum\limits_{n=-\infty}^{\infty} [g(n-u\rho)g^*(n-u\rho)]\, e^{-j2\pi\tilde{\beta}n}, \\ \text{for } \tilde{\tau} = \mu\rho + \text{sgn}(\mu)\tilde{\tau}_s,\ \mu = \pm(M-L+2), \ldots, \pm(M-2), \pm(M+2), \ldots, \\ \pm(M+L-2),\ 0 \le \tilde{\tau}_s < \rho, \text{ and } \tilde{\beta} = b[(M+L)\rho]^{-1},\ b \text{ integer}, \\ 0, \text{ otherwise}, \end{cases} \tag{2.72}$$

where $\tilde{\tau}_s = \frac{\tau_s}{T_s}$ and T_s is the sampling period.

Figs. 2.19 and 2.20 show the magnitude of theoretical and estimated CAF versus

positive delays and at zero CF, respectively, for the SC-FDMA signals in the absence of noise. We consider SC-FDMA signals with a 1.4 MHz double-sided bandwidth, FFT size $N = 64$, IFFT size $M = 128$, $Q = 2$, and 16-QAM modulation with unit variance constellation. The CP duration equals 1/4 of the useful SC-FDMA symbol duration, a root raised cosine pulse shape with a roll-off factor of 0.35 is employed at the transmit-side, $\rho = 4$, a Butterworth low-pass filter of order 13 is used as the receive filter, and observation time equals 20 ms.

Figs 2.21 and 2.22 show the magnitude of theoretical and estimated CAF at zero delay versus cycle frequency, While, Figs. 2.23 and 2.24 depict the magnitude of theoretical and estimated CAF at delay ρ versus cycle frequency.

From these figures, one can easily notice that the estimated CAF magnitude of SC-FDMA signals are in agreement with the theoretical findings. Note that the non-zero values that appear in simulation results, which theoretically are zero, are due to a finite observation time; these are not statistically significant.

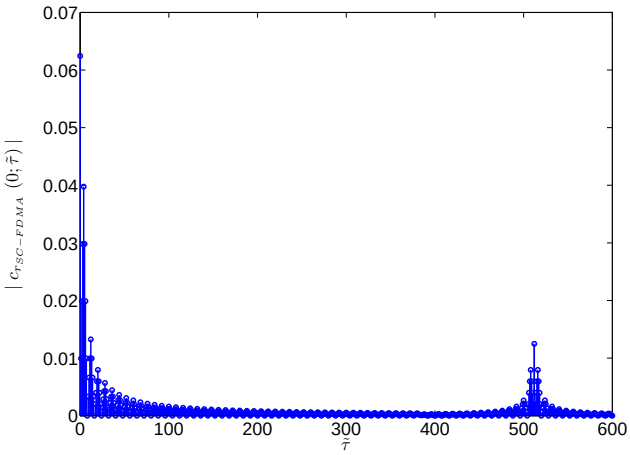

Fig. 2.19: Theoretical results for the CAF magnitude at zero CF ($\tilde{\beta} = 0$) versus positive delays, $\tilde{\tau}$, for SC-FDMA signals.

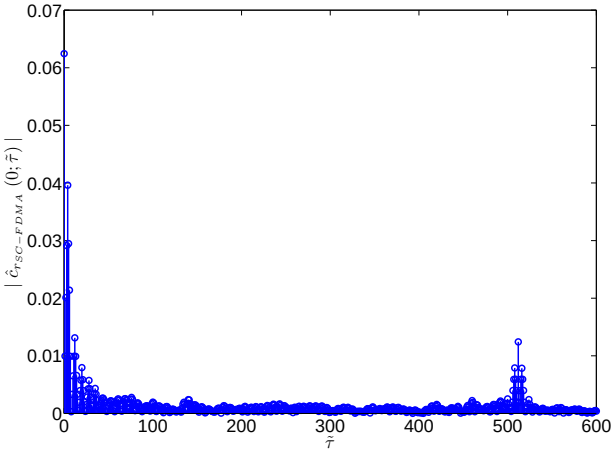

Fig. 2.20: Simulation results for the CAF magnitude at zero CF ($\tilde{\beta} = 0$) versus positive delays, $\tilde{\tau}$, for SC-FDMA signals.

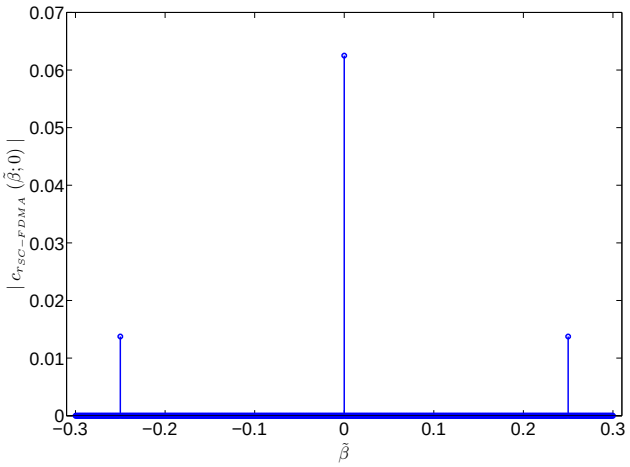

Fig. 2.21: Theoretical results for the CAF magnitude at zero delay ($\tilde{\tau} = 0$) versus cycle frequency , $\tilde{\beta}$, for SC-FDMA signals.

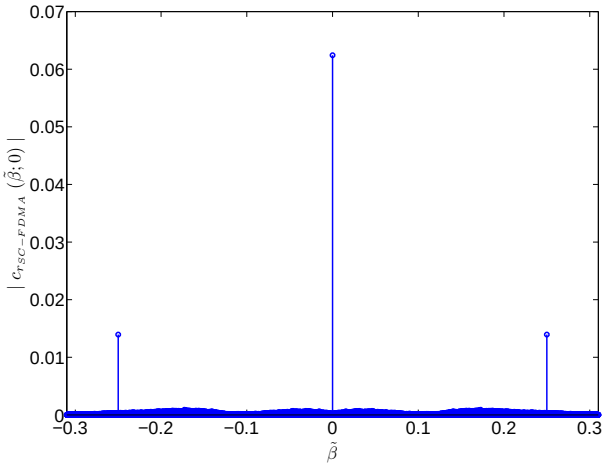

Fig. 2.22: Simulation results for the CAF magnitude at zero delay ($\tilde{\tau} = 0$) versus cycle frequency , $\tilde{\beta}$, for SC-FDMA signals.

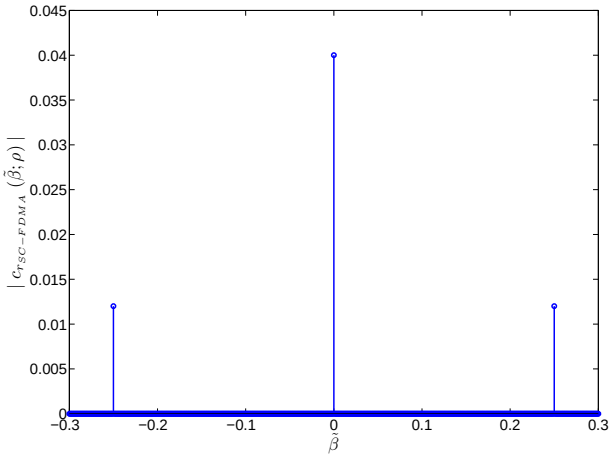

Fig. 2.23: Theoretical results for the CAF magnitude at delay $\tilde{\tau} = \rho$ versus cycle frequency, $\tilde{\beta}$, for SC-FDMA signals.

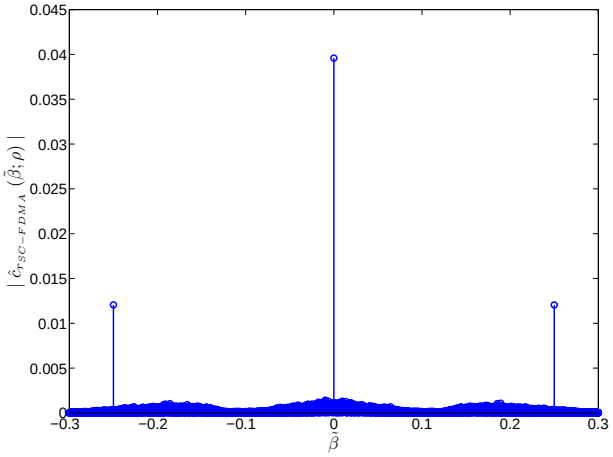

Fig. 2.24: Simulation results for the CAF magnitude at delay $\tilde{\tau} = \rho$ versus cycle frequency, $\tilde{\beta}$, for SC-FDMA signals.

2.6 SC-FDMA Implementation in LTE Uplink

Long Term Evolution (LTE) is the most popular standard that uses SC-FDMA at the physical layer of its uplink (UL) traffic. SC-FDMA signals have been proposed as a promising alternative to orthogonal frequency division multiplexing (OFDM) for UL traffic in LTE due to the lower peak-to-average power ratio (PAPR). On the other hand, they offer the same degree of Inter-symbol interference combat as OFDM [23].

Based on the previous discussion, the basic transmitter architecture of SC-FDMA is very similar to orthogonal frequency division multiple access that is used in LTE downlink (DL). Significantly, because the SC-FDMA waveform is essentially a single-carrier, the PAPR is lower. Therefore, less power consumption occurs in user equipment terminals.

In this section, we describe the physical layer implementation of SC-FDMA in LTE uplink.

2.7 LTE UL Frame and Resource Structure

2.7.1 Generic Frame Structure

An element shared by the LTE DL and UL is the generic frame structure. The LTE specifications define both the frequency division duplex (FDD) and the time division duplex (TDD) modes of operation. This work deals exclusively with describing FDD specifications.

The generic frame structure applies to both the DL and the UL for FDD operation is shown in Fig. 2.25. The frame time duration is 10 msec, and each frame is divided into 20 slots, with the slot duration equal to 0.5 msec. Each subframe contains two slots which yield 1.0 msec.

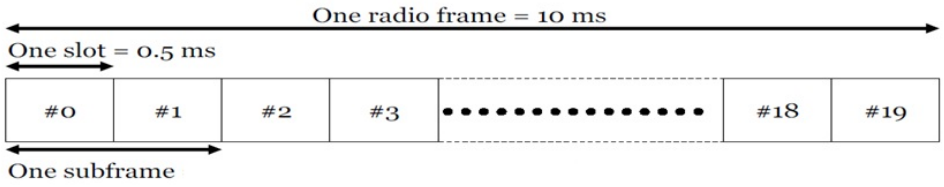

Fig. 2.25: The FDD uplink frame structure in the LTE SC-FDMA-based systems [15].

2.7.2 LTE Uplink Resource Structure

The LTE uplink resource grid for one time slot is illustrated in Fig. 2.26. Each element in the resource grid is called a resource element and is uniquely defined by the index pair (k, l) in a slot, where k and l are the indices in the frequency domain, $k \in \left\{0, 1, 2, ..., N_{RB}^{UL} N_{SC}^{RB} - 1\right\}$, and time domain, $l \in \left\{0, 1, 2, ..., N_{symb}^{UL} - 1\right\}$, respectively. The number of resource block is N_{RB}^{UL}, while N_{SC}^{RB} is the number of subcarriers in a resource block. The consecutive SC-FDMA symbols in the time domain is N_{symb}^{UL}, where N_{symb}^{UL} depends on the CP length and the useful symbol duration. N_{SC}^{RB} equal 12 subcarriers for the LTE signals with a $\triangle f = 15$ kHz subcarrier spacing. Thus, a physical resource block in the uplink consists of $N_{symb}^{UL} \times N_{SC}^{RB}$ resource elements, corresponding to one slot of $N_{symb}^{UL} = 7$ (short CP) or $N_{symb}^{UL} = 6$ (long CP) time domain symbols, and $N_{SC}^{RB} \times \triangle f = 180$ kHz in the frequency domain. The ratio between the CP length and the useful SC-FDMA symbol duration T_{cp}/T_u equals 1/4 for long CP, while for short CP this is 10/128 for the first SC-FDMA symbol in the slot and 9/128 for the remaining SC-FDMA symbols in the slot.

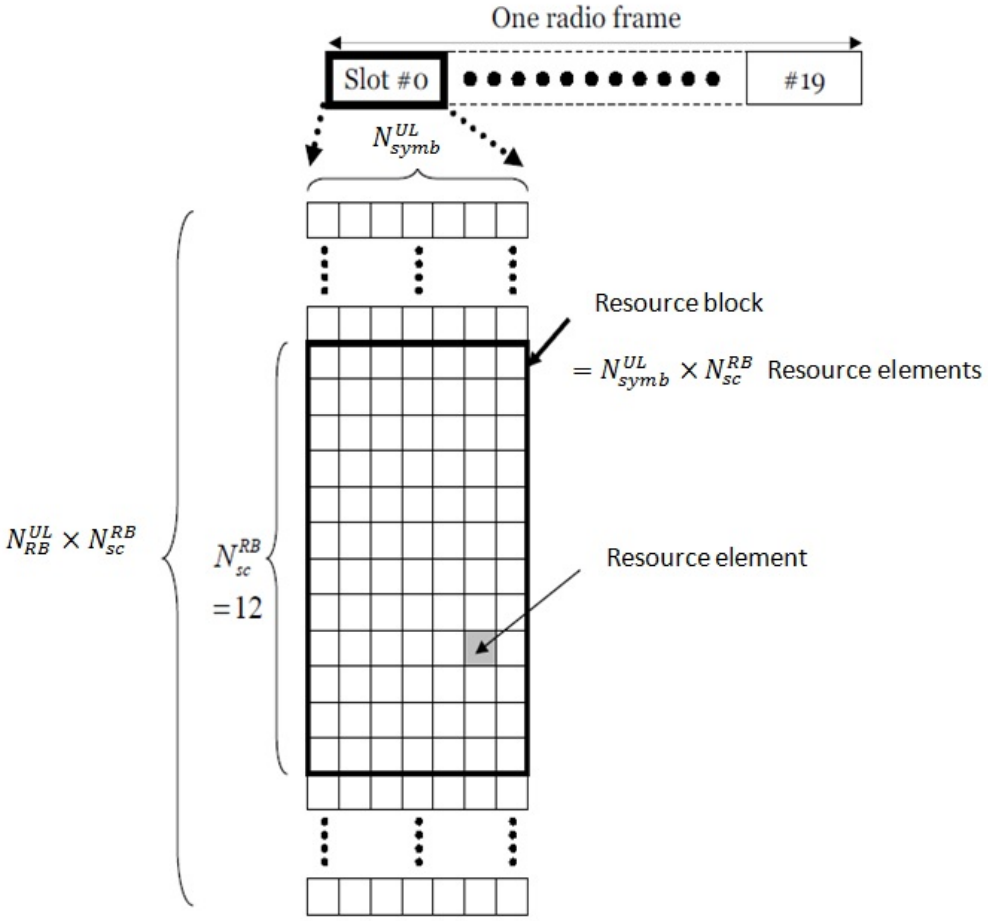

Fig. 2.26: The slot structure and resource grid in the FDD uplink frame [15].

Table 2.1 shows the set of allowed values for resource block numbers, occupied subcarriers and transmission bandwidths.

Table 2.1: LTE SC-FDMA parameters.

Bandwidth (MHz)	1.4	3	5	10	15	20
Number of resource blocks	6	15	25	50	75	100
Number of occupied subcarriers	72	180	300	600	900	1200
IFFT size	128	256	512	1024	1536	2048

2.8 Summary

In this chapter, the signal model of the SC-FDMA signal is provided, the second order cyclostationarity of the SC-FDMA signal is investigated, and closed-form expressions for the CAF and CFs are derived. Furthermore, we compare analytical findings with simulation results, which are in agreement. Finally, a description of the structure of the SC-FDMA-based LTE signals is discussed.

Chapter 3

Proposed Algorithm for the Detection of the LTE SC-FDMA Signals

3.1 Introduction

In this chapter, results obtained in Chapter 2 for the CAF of SC-FDMA signals are exploited to develop a cyclostationarity-based algorithm for their detection. The detection performance is evaluated through computer simulations and laboratory experiments. We first introduce the SC-FDMA signal features, then describe the proposed algorithm, and finally, present the algorithm performance.

3.1.1 Signal Feature Used for Detection

The SC-FDMA signals are detected in the frequency bands allocated to the LTE system [26]; accordingly, the values of M and N are known. The signal is down-converted and oversampled, and the baseband discrete-time signal, $r(u)$, $0 \leq u \leq$

$U_s - 1$, is exploited for detection. Based on the theoretical results presented in Chapter 2, one can see that the CAF magnitude of the received LTE SC-FDMA has the following properties:

- It has non-zero values at CF zero and for delays around $\pm\rho M$, with the latter due to the existence of the CP.
- It is non-zero at CFs equal to $\pm\rho^{-1}$ and for delays around zero.

These particular properties are exploited for the LTE SC-FDMA signal detection. Under hypothesis $\mathcal{H}_1$, we assume that the LTE SC-FDMA is present, while under $\mathcal{H}_0$ it is not.

3.1.2 Cyclostationarity Test Used for Decision-Making

Based on the underlying theory of the cyclostationarity test introduced in [28], which verifies if CAF has a CF at $\tilde{\beta}$ for delay $\tilde{\tau}$, we develop a test for two CFs ($\tilde{\beta_1} = 0$ and $\tilde{\beta_2} = \rho^{-1}$) and two delays ($\tilde{\tau_1} = \rho M$ and $\tilde{\tau_2} = 0$), such that we exploit the above mentioned properties of the LTE SC-FDMA signals.

The test used for decision-making is as follows:

- The CAF of the received signal $r(u)$ is estimated (from U_s samples) at each tested frequency $\tilde{\beta}_i$ and delay $\tilde{\tau}_i$, $i = 1, 2$, and a vector $\hat{c}_i$ is formed as

$$\hat{c}_i = [\mathrm{Re}\{\hat{c}_r(\tilde{\beta}_i; \tilde{\tau}_i)\}\, \mathrm{Im}\{\hat{c}_r(\tilde{\beta}_i; \tilde{\tau}_i)\}], \tag{3.1}$$

where Re {.} and Im {.} are the real and the imaginary parts, respectively.

- A statistic Ψ_i , $i = 1, 2$, is computed for each tested frequency $\tilde{\beta}_i$ and delay $\tilde{\tau}_i$ as [28]

$$\Psi_i = U_s \hat{c}_i \hat{\sum}_i^{-1} \hat{c}_i^{\intercal}, \tag{3.2}$$

where the superscripts -1 and $\intercal$ denote the matrix inverse and transpose, respectively, and $\hat{\sum}_i$ [1] is an estimate of the covariance matrix

$$\sum_i = \begin{bmatrix} \mathrm{Re}\left\{\left(Q_{2,0} + Q_{2,1}\right)/2\right\} & \mathrm{Im}\left\{\left(Q_{2,0} - Q_{2,1}\right)/2\right\} \\ \mathrm{Im}\left\{\left(Q_{2,0} + Q_{2,1}\right)/2\right\} & \mathrm{Re}\left\{\left(Q_{2,1} - Q_{2,0}\right)/2\right\} \end{bmatrix}, \tag{3.3}$$

with

$$Q_{2,0} = \lim_{U_s \to \infty} U_s \mathrm{Cum}[\hat{c}_r(\tilde{\beta}_i; \tilde{\tau}_i), \hat{c}_r(\tilde{\beta}_i; \tilde{\tau}_i)], \tag{3.4}$$

With the CUM[.] as cumulant operator, and

$$Q_{2,1} = \lim_{U_s \to \infty} U_s \mathrm{Cum}[\hat{c}_r(\tilde{\beta}_i; \tilde{\tau}_i), \hat{c}_r^*(\tilde{\beta}_i; \tilde{\tau}_i)]. \tag{3.5}$$

For a zero-mean process, the covariances $Q_{2,0}$ and $Q_{2,1}$ are given respectively as [28]

$$Q_{2,0} = \lim_{U_s \to \infty} U_s^{-1} \sum_{l=0}^{U_s - 1} \sum_{\xi = -\infty}^{\infty} \mathrm{Cum}\left[f\left(l; \tilde{\tau}_i\right), f\left(l + \xi; \tilde{\tau}_i\right)\right] e^{-j2\pi 2\tilde{\beta}_i l} e^{-j2\pi \tilde{\beta}_i \xi}, \tag{3.6}$$

and

$$Q_{2,1} = \lim_{U_s \to \infty} U_s^{-1} \sum_{l=0}^{U_s - 1} \sum_{\xi = -\infty}^{\infty} \mathrm{Cum}\left[f\left(l; \tilde{\tau}_i\right), f^*\left(l + \xi; \tilde{\tau}_i\right)\right] e^{-j2\pi(-\tilde{\beta}_i)\xi l}, \tag{3.7}$$

where $f\left(l; \tilde{\tau}_i\right) = r(l) r^*(l + \tilde{\tau}_i)$ is the second-order (one-conjugate) lag product.

Moreover, the estimators of the covariance $Q_{2,0}$ and $Q_{2,1}$ are given respectively by [28]

[1] Note that although $Q_{2,0}$ and $Q_{2,1}$ depend on i, this dependency was not shown for simplicity of notation.

$$\hat{Q}_{2,0} = (U_s U_{sw})^{-1} \sum_{s=-(U_{sw}-1)/2}^{(U_{sw}-1)/2} W(s) F_{\tilde{\tau}_i}(\tilde{\beta}_i - sU_s^{-1}) F_{\tilde{\tau}_i}(\tilde{\beta}_i + sU_s^{-1}), \tag{3.8}$$

and

$$\hat{Q}_{2,1} = (U_s U_{sw})^{-1} \sum_{s=-(U_{sw}-1)/2}^{(U_{sw}-1)/2} W(s) F^*_{\tilde{\tau}_i}(\tilde{\beta}_i + sU_s^{-1}) F_{\tilde{\tau}_i}(\tilde{\beta}_i + sU_s^{-1}), \tag{3.9}$$

where $W(s)$ is a spectral window of length U_{sw} and $F_{\tilde{\tau}_i}(\tilde{\beta}_i) = \sum_{u=0}^{U_s-1} r(u) r^*(u - \tilde{\tau}_i) e^{-j2\pi\tilde{\beta}_i u}$.

- With the test statistics Ψ_1 and Ψ_2 calculated based on the estimated CAF at $\tilde{\beta}_1 = 0$ and $\tilde{\tau}_1 = \rho M$ and at $\tilde{\beta}_2 = \rho^{-1}$ and $\tilde{\tau}_2 = 0$, respectively, we form a new test statistic, $\Upsilon = \Psi_1 + \Psi_2$. For decision-making, we compare Υ against a threshold, Γ. If $\Upsilon \geq \Gamma$, we decide that the LTE SC-FDMA is present (hypothesis $\mathcal{H}_1$); otherwise, it is not (hypothesis $\mathcal{H}_0$). By using the fact that the statistics Ψ_1 and Ψ_2 have asymptotic chi-square distribution with two degrees of freedom [28], it is straightforward to find that Υ asymptotically follows a chi-square distribution with four degrees of freedom. The threshold Γ is obtained from the tables of this chi-squared distribution for a given value of probability of false alarm (P_{fa}), i.e., $P_{fa} = P_r\{\Psi \geq \Gamma \mid H_0\}$ [29]. A summary of the proposed detection algorithm is provided below.

C. Complexity Analysis of the Proposed Detection Algorithm

The computational complexity of the algorithm is basically determined by the calculation of the test statistic Υ, which entitles computation of Ψ_1 and Ψ_2. In order to obtain the number of operations required for that, in the following we investigate the complexity of estimating the CAF at $\tilde{\beta}_i$ and $\tilde{\tau}_i$, $\hat{c}_r(\tilde{\beta}_i, \tilde{\tau}_i)$, $i = 1, 2,$. As such, according to (2.7), the estimation of CAF at $\tilde{\beta}_1 = 0$ and $\tilde{\tau}_1 = \rho M$ requires U_s complex

Summary of the proposed detection algorithm

Input: The observed samples $r(u)$, $u = 0, ..., U_s - 1$, and ρ, M, and target P_{fa}.
- Calculate $\hat{c}_r(0, \rho M)$ and $\hat{c}_r(\rho^{-1}, 0)$ using (2.7).
- Calculate Ψ_1 using $\hat{c}_r(0, \rho M)$, according to (3.2).
- Calculate Ψ_2 using $\hat{c}_r(\rho^{-1}, 0)$, according to (3.2).
- Calculate $\Upsilon = \Psi_1 + \Psi_2$.
- Calculate Γ based on P_{fa}.

if $\Upsilon \geq \Gamma$ **then**
- LTE SC-FDMA is present ($\mathcal{H}_1$ true).

else
- LTE SC-FDMA is not present ($\mathcal{H}_0$ true).

end if

multiplications and $U_s - 1$ complex additions, while $2U_s$ complex multiplications and $U_s - 1$ complex additions are required for $\tilde{\beta}_2 = \rho^{-1}$ and $\tilde{\tau}_2 = 0$. Furthermore, based on (3.3), (3.8), (3.9), and the expression of Ψ_i in (3.2), one can find that the number of complex multiplications, complex additions, and real operations needed to calculate Ψ_i is $(U_s/2)log_2U_s+2U_{sw}$, $U_slog_2U_s+2(U_{sw}-1)$, and $9U_{sw}+26$, respectively. Moreover, by considering Ψ_1, Ψ_2, Υ, as well as the comparison between Γ and Υ, and using the fact that the number of complex multiplications requires 6 floating point operations (flops), the number of complex additions requires 2 flops, and real operations requires 1 flop, the total number of flops required by the algorithm equals $10U_slog_2U_s + 22U_s + 50U_{sw} + 42$ [2]. For example, with U_s =64000 (12.8 ms observation time) and $U_{sw} = 0.006U_s$, the proposed algorithm requires 11,645,343 flops, while with U_s =32000 (6.4 ms observation time), the proposed algorithm requires 5,502,692 flops. Practically speaking, with a microprocessor that can execute up to 79.2 billion flops per second[3], a decision can be performed in approximately 0.147 ms when the observation time is 12.8 ms and in 0.069 ms when the observation time is 6.4 ms. Apparently, there is a

[2]Note that the common terms which appeared in the computation of the statistic were counted only once.

[3][Online]. Available: http://ark.intel.com/Product.aspx?id=47932&processor=i7-980X&spec-codes=SLBUZ.

tradeoff between complexity and performance, i.e., a longer observation time will lead to an increased complexity, but also to an improved performance, as it will be shown in Section V.

3.2 Simulation and Experimental Results

3.2.1 Simulation Setup

The performance of the algorithm proposed for the detection of the LTE SC-FDMA signals used in the uplink transmission is investigated here. Unless otherwise mentioned, the following parameter values were employed for the SC-FDMA signals [26]: 1.4 MHz bandwidth, $N = 72$, $M = 128$, $\rho = 4$. The subcarrier spacing was set to $\triangle f = 15$ kHz, L/M =1/4 for long CP, and L/M=10/128 for the first symbol in the slot and L/M =9/128 for the remaining symbols for short CP. An RRC with 0.35 roll-off factor was employed at the transmit-side and 16-QAM modulation with unit variance was considered. The impairments which affected the received signals were: 500 kHz carrier frequency offset and uniformly distributed phase and timing offsets over $[-\pi, \pi)$ and $[0, 1)$, respectively. We considered the additive white Gaussian noise (AWGN), and ITU-R pedestrian and vehicular A channels [30]. The maximum Doppler frequencies equal 9.72 Hz and 194.44 Hz for the pedestrian and vehicular fading channels, respectively. The out-of-band noise was removed at the receive-side with a 13 order low-pass Butterworth filter, and the SNR was set at the output of this filter. The probability of detection P_d, is used as a performance measure; this is estimated based on 1000 Monte Carlo trials. Unless otherwise mentioned, the sensing times of 6.4 ms and 12.8 ms were used, and the probability of false alarm was equal to P_{fa}= 0.01.

3.2.2 Experimental Setup

A measurement station was set up as depicted in Fig. 3.1. This consists of: 1) a processing and control unit, namely, a personal computer (PC), 2) an Agilent vector signal generator (VSG N5182A), and 3) a Keithley vector signal analyzer (VSA 2080). The three components were interfaced via Ethernet. By using the LTE SC-FDMA signal emulation built into the VSG and the Agilent Studio toolkit, the VSG generated an RF analog signal, which was transmitted to the VSA through a cable. The received analog RF signal was down-converted to intermediate frequency, and then converted to a digital signal, as well as to baseband. Finally, by using the Keithley SignalMeister, the signal captured with the VSA was transferred to the PC, where the detection algorithm was applied. The signal parameters were the same as used in the computer simulations.

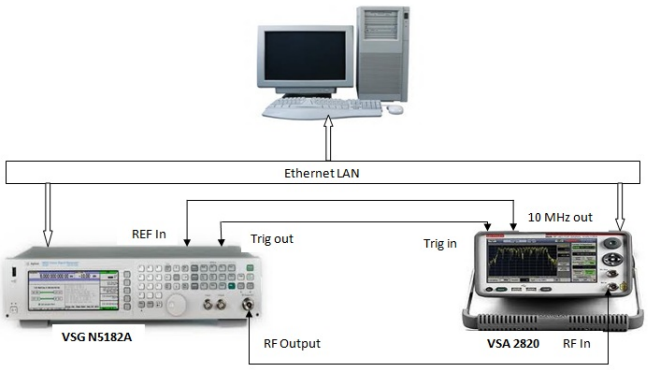

Fig. 3.1: Measurement station.

3.2.3 Algorithm Performance

The performance of the proposed algorithm is investigated in terms of the probability of detection, P_d, for the LTE SC-FDMA signals. This probability is plotted versus the probability of false alarm, P_{fa}, in Fig. 3.2, while it is depicted versus SNR in

Figs. 3.3-3.6. Results obtained from both computer simulations (black color) and experiments (red color) are shown, for the AWGN (solid line), ITU-R pedestrian A (dashed line), and ITU-R vehicular A fading (dashed-dot line) channels. As can be easily seen, there is a very good agreement between experimental and simulation findings.

In Fig. 3.2, results for P_d versus P_{fa} are presented at different SNRs, for the ITU-R pedestrian A fading channel and with 12.8 ms observation time. Clearly, the detection performance improves with an increase in SNR. For example, with -10 dB SNR, P_d reaches 1 at P_{fa} around 0.1, while with -5 dB SNR, this occurs at P_{fa} around 0.35. Fig. 3.3 shows P_d versus SNR for the LTE SC-FDMA signal with long CP, and considering the three channels, as well as the observation times of 6.4 ms and 12.8 ms. As expected, the best performance is obtained in the AWGN channel, followed by the pedestrian and vehicular A channels. While results achieved in the pedestrian A channel are close to those in AWGN, a longer observation time is required to reach the same performance in the vehicular A channel. Also as expected, P_d improves as the observation time increases. Fig. 3.4 depicts P_d versus SNR for the vehicular A channel, with different observation times. As previously noticed, the detection performance enhances with an increase in the observation time. Fig. 3.5 presents the detection performance for LTE SC-FDMA signals with long and short CPs for the pedestrian and vehicular A channels. As expected, a reduction in the CP duration adversely affects the performance under the same conditions. This is explained by the reduction in the correlation resulting from the reduced CP duration. Furthermore, we investigate P_d versus SNR for different oversampling factors ρ in Fig. 3.6 for the pedestrian A channel, with observation times of 6.4 ms and 12.8 ms. As expected, the detection performance improves with an increase in ρ for a certain observation time, as the number of samples increase, which in turn leads to more accurate estimates. Fig.

3.7 presents the performance of signal detection for 1.4 MHz ($N = 72, M = 128$) and 5 MHz ($N = 300, M = 512$) LTE SC-FDMA signals versus SNR. As can be noticed, the performance is better in the latter case, as an increased number of samples is achieved over a certain observation time with a given oversampling factor, which in turn leads to more accurate estimates.

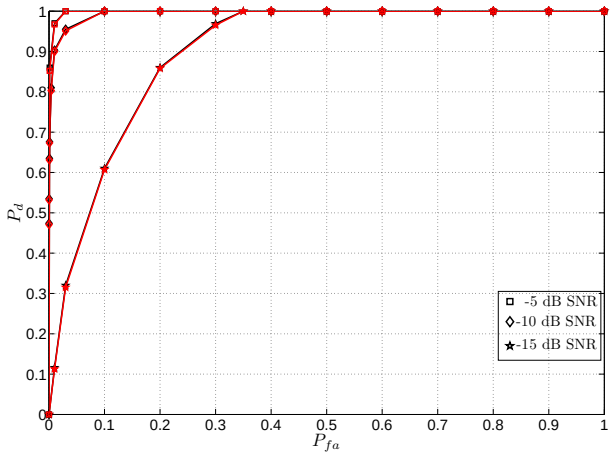

Fig. 3.2: The probability of detection versus P_{fa} for LTE SC-FDMA signals with long CP propagation through pedestrian A channel for different SNRs with 12.8 ms observation time. Simulation (black color) and experimental (red color) results.

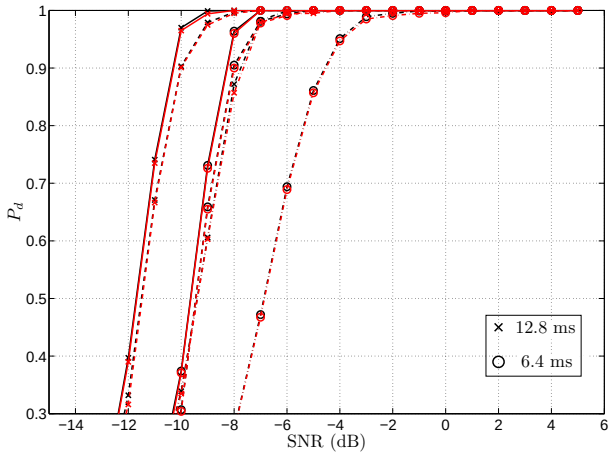

Fig. 3.3: The probability of detection versus SNR for the LTE SC-FDMA signals with long CP affected by AWGN (solid line), pedestrian A (dashed line), and vehicular A (dashed-dot line) channels, respectively. Simulation (black color) and experimental (red color) results.

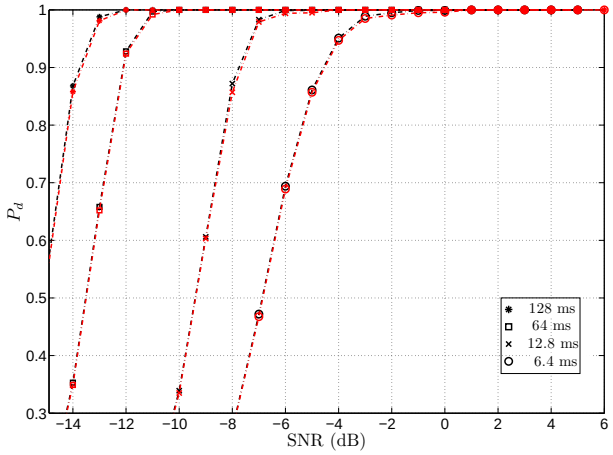

Fig. 3.4: The probability of detection versus SNR for LTE SC-FDMA signals with long CP propagation through vehicular A channel for different observation times. Simulation (black color) and experimental (red color) results.

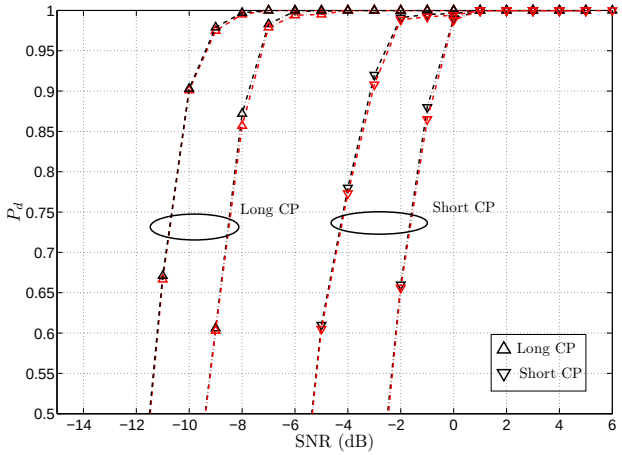

Fig. 3.5: The probability of detection versus SNR for LTE SC-FDMA signals with long and short CP propagating through pedestrian A (dashed line) and vehicular A (dashed-dot line) channels with 12.8 ms observation time. Simulation (black color) and experimental (red color) results.

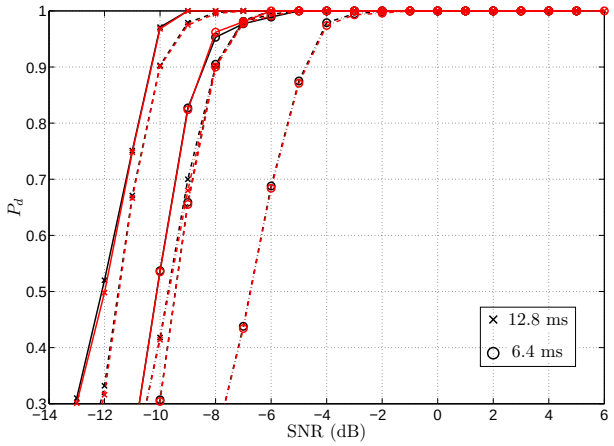

Fig. 3.6: The probability of detection versus SNR for the LTE SC-FDMA signals with long CP affected by pedestrian A channel, when $\rho = 8$ (solid line), 4 (dashed line), and 2 (dashed-dot line). Simulation (black color) and experimental (red color) results.

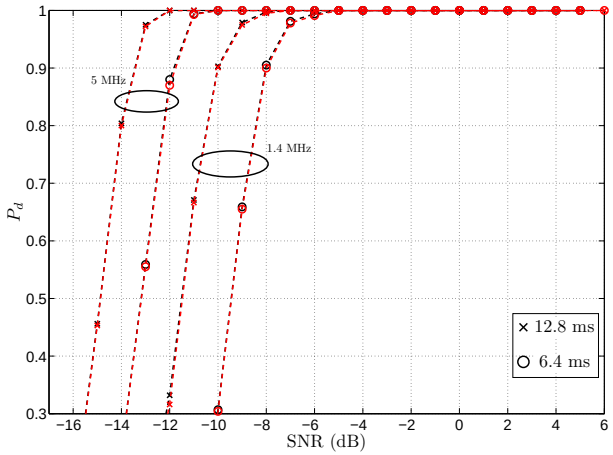

Fig. 3.7: The probability of detection for the 1.4 MHz LTE SC-FDMA and 5 MHz LTE SC-FDMA signals versus SNR with long CP affected by pedestrian A channel. Simulation (black color) and experimental (red color) results.

3.3 Summary

In this chapter, an algorithm based on the second-order cyclostationarity was developed for the detection of SC-FDMA signals. Experiments were carried out using computer simulations and signals generated by laboratory equipment to evaluate the performance of the proposed algorithm under diverse scenarios, involving various channel conditions, SNRs, and observation times. The algorithm does not require frequency and timing synchronization, and estimation of signal and noise power. The algorithm can be implemented in real time, with a tradeoff between complexity and performance.

Chapter 4

Classification of SC-FDMA, OFDM, and SC Signals

4.1 Introduction

In this chapter we develop an algorithm to classify SC-FDMA, OFDM and SC signals based on their second-order cyclostationarity. The results obtained in Chapter 2 for the CAF of the SC-FDMA signal are exploited to develop this algorithm. We first introduce the discriminating signal features, then describe the proposed algorithm, and finally present the algorithm performance.

4.2 Proposed Signal Classification Algorithm

Based on the theoretical results presented in Chapter 2, we can draw the following conclusions on the CAF magnitude of the SC-FDMA signal:

- The CAF magnitude has non-zero values at delays around zero and $\pm\rho M$, with the latter due to the existence of the CP.

- The CAF magnitude is non-zero at CFs equal to $\pm\rho^{-1}$ and for delays around zero, as well as at CFs integer multiples of $[(M+L)\,\rho]^{-1}$ and for delays around a $\pm\rho M$.

Based on the second-order cyclostationrity features of OFDM and SC signals [16], we can draw the following conclusion on the CAF magnitude of the OFDM and SC signals:

- The CAF magnitude of OFDM signals has non-zero values at delays around zero and $\pm\rho K$, with the latter due to the existence of the CP. Here K represents the number of subcarriers.

- For OFDM signals, the CFs are integer multiples of D^{-1}, where $D = \rho K(1 + T_{cp}T_u^{-1})$, with T_{cp} and T_u as the CP duration and useful symbol duration, respectively.

- For SC signals, the CAF magnitude is non-zero at CFs equal to $\pm\rho^{-1}$ and for delays around zero.

These properties are exploited to identify the SC-FDMA signal versus the OFDM and SC. In the bandwidth of interest and after down-conversion, oversampling at rate ρ times the bandwidth is carried out. The corresponding binary decision tree algorithm is presented in Fig. 4.1. At Node 1, we discriminate SC-FDMA and OFDM versus SC signals, and at Node 2 we identify SC-FDMA versus OFDM signals. At each node, a test static is estimated based on the corresponding CAF and compared with a decision threshold [28].

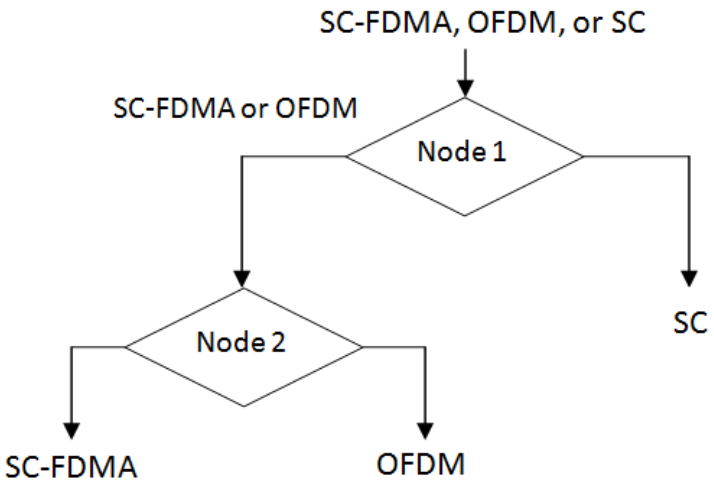

Fig. 4.1: The flowchart of the proposed algorithm for signal classification.

4.3 Classification Performance of the Proposed Algorithm

In this section, the joint detection and classification performance of the proposed algorithm is evaluated through computer simulation and using waveforms generated and acquired by laboratory instrumentation.

4.3.1 Simulation Setup

SC-FDMA, OFDM, and SC signals were considered with a 16-QAM constellation with unit variance. Unless otherwise mentioned, the following parameters values were employed for the SC-FDMA: double-sided bandwidth $B = 1.4$ MHz, $N = 72$, $M = 128$, subcarrier spacing $\triangle f = 15$ kHz, T_{cp}/T_u =1/4 for long CP, and for short CP T_{cp}/T_u =10/128 for the first symbol in the slot and T_{cp}/T_u= 9/128 for the remaining symbols. Note that the LTE standard was followed for parameter set-up. Furthermore, the OFDM and SC signals used a bandwidth $B = 1.25$ MHz. For the

OFDM signal $K = 128$ and T_{cp}/T_u =1/4. The root raised cosine pulse shape with a roll-off factor 0.35 was used at the transmit-side for SC-FDMA and SC signals, and the root cosine window with 0.025 roll-off factor was utilized for the OFDM signals. The impairments which affected the received signals were: 500 kHz carrier frequency offset and uniformly distributed phase and timing offsets over [-π,π) and [0,1), respectively. The considered channels were AWGN and ITU-R pedestrian and vehicular A fading [30], with the delay spread profile of the fading channels specified in Table 4.1. The Jakes's model was used to generate multipath fading [31]. The maximum Doppler spread of the pedestrian and vehicular fading channels were 9.72 Hz and 194.44 Hz, respectively. The out-of-band noise was removed at the receive-side with a 13 order low-pass Butterworth filter, and the SNR was set at the output of this filter. Observation times of 6.4 ms and 12.8 ms were used, and the decision threshold was set to 19.807 at Node 1 and 18.42 at Node 2. The probability of correct classification $P_{cc}(i|i)$, i = SC-FDMA, OFDM, and SC, were obtained from 1,000 Monte Carlo simulation.

Table 4.1: Tapped-delay-line implementation of ITU-R models [30].

	Pedestrian A channel		Vehicular A channel	
Tap no.	Delay (ns)	Power (dB)	Delay (ns)	Power (dB)
1	0	0	0	0
2	110	-9.7	310	-1
3	190	-19.2	710	-9
4	410	-22.8	1090	-10
5	NA	NA	1730	-15
6	NA	NA	2510	-20

4.3.2 Algorithm Performance

The probability of correct classification, $P_{cc}(i|i)$, i = SC-FDMA, OFDM, and SC are respectively plotted versus SNR in Figs. 4.2-4.6 based on computer simulation (black colors) and experiments (red colors). Three channels are considered: AWGN (solid line), ITU-R pedestrian A (dashed line), and ITU-R vehicular A (dash-dot line), for the observation times of 6.4 ms and 12.8 ms. As can be seen, there is a very good agreement between experimental and simulation results. Regardless of the sensing time, the SC-FDMA with long CP and SC classification performance is similar for the AWGN and pedestrian fading channels, but degrades for the vehicular fading channels. For the latter case, neither 6.4 ms nor 12.8 ms is sufficient to provide an acceptable performance regardless of the SNR. Fig. 4.4, for the 12.8 ms observation time, the OFDM classification performance is similar for all three channels. On the other hand, for the 6.4 ms sensing time, the performance has a similar behavior as for SC-FDMA and SC.

Moreover, we investigated the effect of the observation time on the classification performance for SC-FDMA signals with long CP in Fig. 4.5. As can be noticed, a longer sensing time is required to attain a reasonable performance. For example, 256 ms is needed to achieve a probability of correct classification approaching one at around 9 dB SNR. Fig. 4.6 presents the classification performance for SC-FDMA signals with long and short CPs. As expected, a reduction in the CP duration adversely affects the classification performance under the same conditions. This is explained by the reduction in the correlation resulting from the reduced CP duration. Both simulation and experimental results are in agreement.

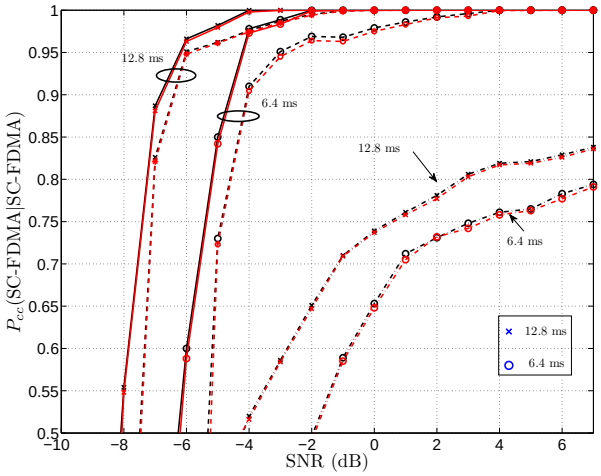

Fig. 4.2: The probability of correct classification versus SNR for SC-FDMA signals with long CP affected by AWGN (solid line), ITU-R pedestrian A (dashed line), and vehicular A (dashed-dot line) fading channels, respectively.

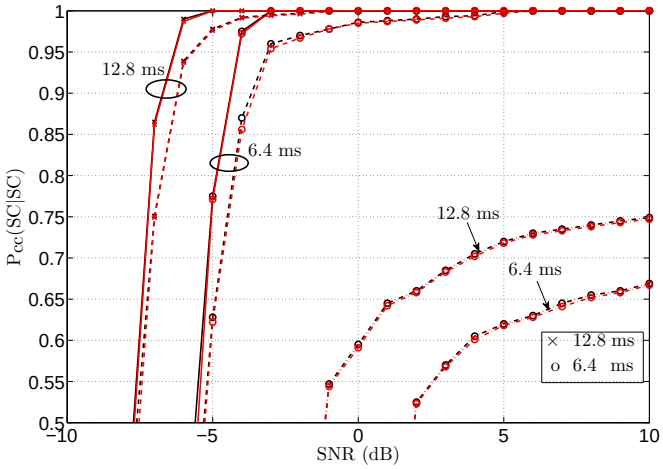

Fig. 4.3: The probability of correct classification versus SNR for SC signals propagation through AWGN (solid line), ITU-R pedestrian A (dashed line), and vehicular A (dashed-dot line) fading channels.

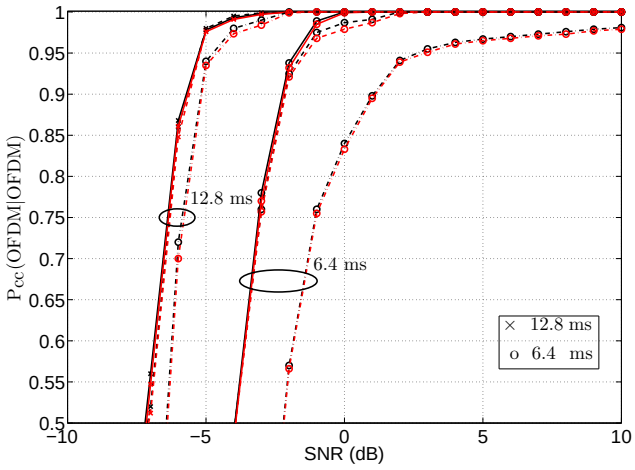

Fig. 4.4: The probability of correct classification versus SNR for OFDM signals propagation through AWGN (solid line), ITU-R pedestrian A (dashed line), and vehicular A (dashed-dot line) fading channels.

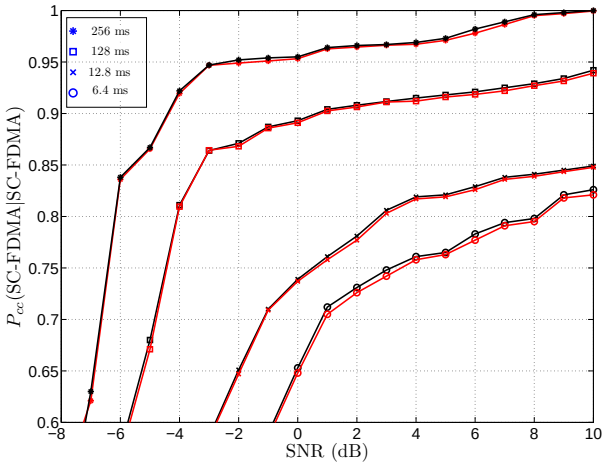

Fig. 4.5: The probability of correct classification versus SNR for SC-FDMA signals with long CP propagation through vehicular A fading channels for different observation times.

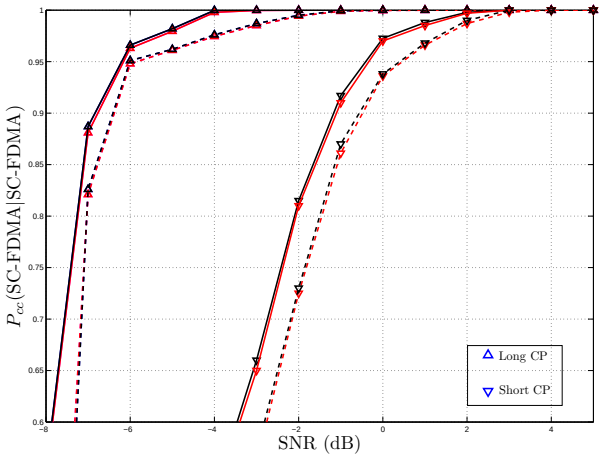

Fig. 4.6: The probability of correct classification versus SNR for SC-FDMA signals with long and short CP propagation through AWGN (solid line), ITU-R pedestrian A (dashed line) fading channels with 12.8 ms observation time.

The confusion matrix shown in Table 4.2 and Table 4.3 for SC-FDMA with long CP and SC-FDMA with short CP, respectively, for 12.8 ms observation time and -2 dB SNR in pedestrian A channel further illustrate the classification performance.

Table 4.2: Confusion matrix for 12.8 ms observation time and -2 dB SNR in ITU-R pedestrian A channel with using SC-FDMA (long CP).

Transmitted / Decision	SC-FDMA (long CP)	OFDM	SC
SC-FDMA (long CP)	994	5	1
OFDM	0	1000	0
SC	3	1	996

Table 4.3: Confusion matrix for 12.8 ms observation time and -2 dB SNR in ITU-R pedestrian A channel with using SC-FDMA (short CP).

Transmitted / Decision	SC-FDMA (short CP)	OFDM	SC
SC-FDMA (short CP)	730	194	76
OFDM	0	1000	0
SC	0	2	998

4.4 Summary

In this chapter, an algorithm based on the second-order cyclostationarity was developed for the classification of SC-FDMA, OFDM, and SC signals. Experiments were carried out using computer simulations and signals generated by laboratory equipment to evaluate the performance of the proposed algorithm under diverse scenarios, involving various channel conditions, SNRs, and observation times. The algorithm does not require frequency and timing synchronization, and estimation of signal and noise power. A good performance was obtained at relatively low SNRs and with a relatively short observation time.

Chapter 5

Conclusions and Future Work

In this thesis, the second-order cyclostationarity of SC-FDMA-based signals, which are employed in the uplink LTE, is studied. Furthermore, this is exploited to develop two algorithms for signal detection and classification, respectively, which exhibit a good performance.

The following are the major contributions of this thesis:

- The SC-FDMA signal is studied and mathematically modelled.

- The second-order cyclostationarity of the SC-FDMA signal is investigated, and closed-form expressions for the CAF and CFs are derived.

- These findings are used to select discriminating signal features and develop algorithms for detection and classification of SC-FDMA signals, respectively.

- The detection and the classification performance of the proposed algorithms are evaluated first through computer simulations. The algorithms have the advantage of avoiding the need for frequency and timing synchronization, and estimation of signal and noise powers.

- Experiments are additionally conducted to verify the theoretical findings and the simulation outcomes. These involve an Agilent vector signal generator (VSG N5182A) and a Keithley vector signal analyzer (VSA 2080). Results from experiments agreed with theoretical and simulation results, providing a strong support for the developments introduced in this thesis.

5.1 Future work

While LTE SC-FDMA signals are considered in this thesis, in the LTE standard there is supplementary information, such as preambles and pilots, which induces second-order cyclostationarity and provides additional discriminating features that can be used for signal detection and classification. This leads to a more complex signal model, which is planned to be investigated in future work. In addition, cooperative techniques will be exploited for signal detection and classification. Instead of considering a single reading for each CR, different CRs can share their measurements to improve the detection/classification. Moreover, the applicability of the signal features for parameter estimation will be studied. Recently, multiple-input multiple-output (MIMO) systems have been included in advanced standards of wireless systems, e.g., LTE Advanced. The problem of detecting SC-FDMA in MIMO scenarios is a topic of interest, which will be investigated in the future.

References

[1] I. Akyildiz, W. Lee, M. Vuran, and S. Mohanty, "Next generation/dynamic spectrum access/cognitive radio wireless networks: a survey," *Computer Networks: The International Journal of Computer and Telecommunications Networking*, vol. 50, no. 13, pp. 2127–2159, 2006.

[2] D. Cabric, "Cognitive radio: System design prespective," *Ph.D thesis, University of California, Berkeley*, 2007.

[3] S. Haykin, "Cognitive radio: brain-empowered wireless communications," *IEEE J. Select. Areas Commun.*, vol. 23, pp. 201–220, Feb. 2005.

[4] J. M. III, "Cognitive radio: An integrated agent architecture for software defined radio," *PhD thesis, KTH Royal Institute of Technology*, 2000.

[5] H. Arslan and T. Yücek, *Cognitive Radio, Software Defined Radio, and Adaptive Wireless Systems (Signals and Communication Technology)*. Springer-Verlag New York, Inc., Secaucus, NJ, 2007.

[6] A. Ghasemi and E. Sousa, "Collaborative spectrum sensing for opportunistic access in fading environments," in *IEEE DySPAN*, 2005, pp. 131–136.

[7] D. Cabric, S. Mishra, and R. Brodersen, "Implementation issues in spectrum sensing for cognitive radios," in *Proc. IEEE ASILOMAR*, 2004, pp. 772–776.

[8] S. M. Mishra, S. ten Brink, R. Mahadevappa, and R. W. Brodersen, "Cognitive technology for Ultra-Wideband/WiMax coexistence," in *Proc. IEEE DySPAN*, 2007, pp. 179–186.

[9] Z. Lei and F. Chin, "WiMax signal detection," in *IEEE MILCOM*, 2008, pp. 1–7.

[10] A. Al-Habashna, O. A. Dobre, R. Venkatesan, and D. C. Popescu, "Second-order cyclostationarity of mobile WiMAX and LTE OFDM signals and application to spectrum awareness in cognitive radio systems," *IEEE J. Sel. Topics Sig. Proc.*, vol. 6, pp. 26–42, Feb. 2012.

[11] "IEEE Std 802.11a, part11: Wireless LAN medium access control (MAC) and physical layer (PHY) specifications: high-speed physical layer in the 5 GHz band," Sept. 1999.

[12] H. Myung, J. Lim, and D. Goodman, "Peak-to-average power ratio of single carrier fdma signals with pulse shaping," in *IEEE 17th International Symposium on Personal, Indoor and Mobile Radio Communications*, 2006, pp. 1–5.

[13] H. Ekstrom, A. Furuskar, J. Karlsson, M. Meyer, S. Parkvall, J. Torsner, and M. Wahlqvist, "Technical solutions for the 3g long-term evolution," *IEEE Commun. Mag.*, vol. 44, pp. 38–45, Mar. 2006.

[14] 3rd Generation Partnership Project (3GPP), "Requirements for E-UTRA and E-UTRAN," http://www.3gpp.org/ftp/Specs/htmlinfo/25913.htm.

[15] ——, "Technical specification group radio access network; physical layer aspects for E-UTRA," http://www.3gpp.org/ftp/Specs/html-info/25814.htm.

[16] A. Punchihewa, Q. Zhang, O. A. Dobre, C. Spooner, S. Rajan, and R. Inkol, "On the cyclostationarity of ofdm and single carrier linearly digitally modulated

signals in time dispersive channels: Theoretical developments and application," *IEEE Trans. Wireless Commun.*, vol. 9, pp. 2588–2599, Mar. 2010.

[17] A. Bouzegzi, P. Ciblat, and P. Jallon, "New algorithms for blind recognition of ofdm based systems," *Elsevier Signal Processing*, vol. 90, pp. 900–913, Sep. 2010.

[18] P. Sutton, K. Nolan, and L. Doyle, "Cyclostationary signatures in practical cognitive radio applications," *IEEE J. Sel. Areas Commun.*, vol. 26, pp. 13–24, Jan. 2008.

[19] F. Socheleau, P. Ciblat, and S. Houcke, "OFDM system identification for cognitive radio based on pilot-induced cyclostationarity," in *IEEE WCNC*, 2009, pp. 1–6.

[20] O. Dobre, A. Abdi, Y. Bar-Ness, and W. Su, "Survey of automatic modulation classification techniques: classical approaches and new trends," *IET Commun.*, vol. 1, pp. 137–156, Apr. 2007.

[21] M. Shi, A. Laufer, Y. Bar-Ness, and W. Su, "Fourth order cumulants in distinguishing single carrier from ofdm signals," in *IEEE MILCOM*, 2008, pp. 1–6.

[22] D. Grimaldi, S. Rapuano, and L. De Vito, "An automatic digital modulation classifier for measurement on telecommunication networks," *IEEE Trans. Instrum. Meas.*, vol. 56, pp. 1711–1720, Oct. 2007.

[23] H. Myung, J. Lim, and D. Goodman, "Single carrier fdma for uplink wireless transmission," *IEEE Veh. Technol. Mag.*, vol. 1, pp. 30–38, Sep. 2006.

[24] H. G. Myung and D. Goodman, *Single carrier FDMA: a new air interface for long term evolution.* Wiley, 2008, vol. 8.

[25] J. G. Andrews, A. Ghosh, and R. Muhamed, *Fundamentals of WiMAX: understanding broadband wireless networking.* Prentice Hall PTR, 2007.

[26] *Evolved Universal Terrestrial Radio Access (E-UTRA); User Equipment (UE) Radio Transmission and Reception*, 3GPP TS 36.101, 2009.

[27] C. Spooner and W. Gardner, "The cumulant theory of cyclostationary time-series. ii. development and applications," *IEEE Trans. Signal Process.*, vol. 42, no. 12, pp. 3409–3429, Dec. 1994.

[28] A. V. Dandawate and G. B. Giannakis, "Statistical tests for presence of cyclostationarity," *IEEE Trans. Sig. Proc.*, vol. 42, pp. 2355–2369, Sep. 1994.

[29] M. Abramowitz and I. A. Stegun, *Handbook of Mathematical Functions: with Formulas, Graphs, and Mathematical Tables.* Courier Dover Publications, 2012.

[30] A. Molisch, *Wireless Communications.* Wiley, 2011.

[31] H. Harada and R. Prasad, *Simulation and software radio for mobile communications.* Artech House on Demand, 2002.